Metal Halide Analogues of Chalcogenides: A Building Block Approach to the Rational Synthesis of Solid-State Materials

James D. Martin,* Andrew M. Dattelbaum, Todd A. Thornton, Roger M. Sullivan, Jincai Yang, and Michael T. Peachey

Department of Chemistry, North Carolina State University, Raleigh, North Carolina 27695-8204

Received April 8, 1998. Revised Manuscript Received July 2, 1998

Principles of solid-state structure and bonding that relate metal-halide and metal-chalcogenide materials are described through a comparison of binary AX_n salts. Structural variation is rationalized by a comparison of the size and charge of the respective ions, the d-electron count of the cations, and the type of A−X, A−A, and X−X bonding interactions. These general bonding considerations are exploited for the construction of new metal-halide structure types that are patterned after known chalcogenide structures such as metal-halide analogues of silicates, aluminosilicates, phosphates, and phosphonates.

Contents

Introduction

An overview of solid-state chemistry, such as that extracted from the Inorganic Crystal Structure Database (ICSD) summarized in Figure 1, finds metal oxides to be by far the dominant class of inorganic materials. Oxides exhibit widely diverse application such as high-temperature superconductors, optical materials, and catalysts.[1,2] Solid-state non-oxide systems, though significantly underexplored, provide a similarly rich chemistry. With the increasing demand to design materials for specific applications, it is worthwhile to consider the utilization of principles of solid-state structure and bonding that can be gleaned from the plethora of oxide materials for the design and construction of novel non-oxide materials. Others have previously reviewed the chemistry of halides.[3−9] In this review, we articulate foundational structural relationships between chalcogenides and non-chalcogenide materials and demonstrate the application of such principles to the specific construction of a variety of metal-halide materials.

We have recently initiated syntheses of metal-halide framework materials in order to exploit the reactivity of metal-halide building blocks for potential catalytic applications and the polarizablity of the building blocks for potential optical and ion transport applications.[10,11] While the stability of the thermodynamically favored metal oxides provide a robust support for chemistry, the stability comes at the expense of reactivity and mobility. By contrast, textbooks describing organic synthesis will list any variety of metal halides such as CuCl, $FeCl_2$, $ZnCl_2$, $AlCl_3$, $PdCl_2$, $TiCl_4$, $MgCl_2$ $MnCl_2$, $NiCl_2$, ... over the reaction arrow indicating their catalytic function. However, such metal halides are generally used "off the shelf", with little attention paid to the structure of the material. Designs with structural features known for oxide materials that are constructed utilizing reactive and polarizable metal halides can be envisioned as what others have called "solid-state inorganic enzymes".[12]

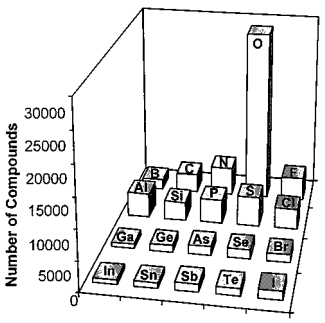

Figure 1. Schematic overview of inorganic compounds from the Inorganic Crystal Structure Database.

Our discussion is focused primarily on the structural and bonding relationships of chlorides and bromides to the oxides and sulfides. These halides and chalcogenides are chosen because their similarity in size and electronegativity results in the greatest commonality of structure. The electronegativities of Cl (3.0) and Br (2.8) are intermediate between O (3.5) and S (2.5), whereas F (4.0) is outside the range of chalcogenides. With respect to size, the covalent radius of O (0.74 Å) is close to that of F (0.72 Å), S (1.04 Å) is similar to Cl (0.99 Å), and Br (1.14 Å) is close to Se (1.17 Å).[13] We limit our discussion to crystallographically characterized materials that exhibit extended structures, though similar comparisons can be made for molecular species.

Construction Principles Derived from Simple AX_n Salts

It has been stated in jest that if you work hard enough, the structure of all solid-state materials can be

10.1021/cm9802550 CCC: $15.00
Published on Web 10/02/1998

Table 1. NaCl Structure Types

I/VII	II/VI	III/IV	IV/IV
LiF, LiCl, LiBr, LiI			
NaF, NaCl, NaBr, NaI	MgO, MgS		
KF, KCl, KBr, KI	CaO, CaS, CaSe, CaTe	ScN, ScP, ScAs, ScSb	TiC
RbF, RbCl, RbBr, RbI	SrO, SrS, SrSe, SrTe	YN, YP, YAs, YSb	ZrC
CsF	BaO, BaS, BaSe, BaTe	LaN, LaP, LaAs, LaSb	HfC

related to sodium chloride or perovskite. This overgeneralization emerges from an understanding of crystal structures derived from the closest packing of spheres. Such packing arguments, dictated by the sizes of the components, are most helpful to describe the ionic bonding limit or also when packing molecular units with no strong intermolecular interactions. Introduction of the directionality of covalent bonding serves to significantly increase the complexity of extended structures. Nevertheless, a majority of structural differentiation can be understood from a consideration of the size, charge, and electron configuration of the components of a crystal structure. In the context of this review of halide/chalcogenide analogues, the charge and electron count of the building blocks are of greatest import, since anions of similar size are considered. Although application of the structural preferences of building blocks to the preparation of complicated structures is shown to be useful for the design of new materials, the commonality of bonding preferences of building blocks provides no guarantee that analogous extended solids can be constructed. This in part lies to the art of the synthetic chemist and to the blessing of nature.

Charge Matching. Charge matching strategies have been widely utilized for the preparation of new materials based on a given structural archetype. Zeolitic materials represent a classic example whereby any variety of framework tetrahedral cations can be substituted into a silicate lattice (Si_mO_{2m}) such that charge neutrality is maintained. This is achieved exclusively by framework cation substitution in the aluminophosphates, $Al_mP_mO_{4m}$, and also by the addition of extra-framework cations in aluminosilicates $[A]_n[Al_nSi_{m-n}O_{2m}]$[14] or cobalt phosphates $[A]_x[Co_xAl_{m-x}P_mO_{4m}]$.[15] Charge matching strategies are similarly useful for the commercially important magnetic oxides with the spinel structure, AB_2O_4, in which the sum of the charges of the A and B cations must balance the −8 charge of the anions as observed for $MgAl_2O_4$, Mg_2TiO_4, $LiAlTiO_4$, $Li_{0.5}Al_{2.5}O_4$, $LiNiVO_4$, and Na_2WO_4.[16] Charge matching strategies by anion substitution are also possible, but much less exhaustively utilized. Halide spinel structures are known for several fluorides, such as Li_2NiF_4. However, in AB_2F_4 structures only +1 and +2 cations are possible, whereas cations with charges of +1 to +6 are observed for the oxides. Cation combinations of +2/+5, +4/+4, and +6/+3 could potentially yield nitride spinel structures; however, forcing the highly charged cations into a tetrahedral site is not generally favored.[17]

Charge matched variations of both anions and cations are readily characterized by consideration of the periodic table. Substitution of a halide anion for an oxide anion (a move to the right on the periodic table) must be compensated by a concurrent move to the left on the periodic table in the choice of a cation. This is clearly demonstrated by the isostructural and approximately isoelectronic series: ReO_3, TaO_2F, $TiOF_2$, ScF_3. The opposing progression across the periodic table for anion and cation variation in a given structure type is clearly apparent for the sodium chloride structure type as demonstrated in Table 1. Group 1 halides, group 2 chalcogenides, group 3 pnictides, and group 4 tetrelides all adopt this common structure. The charge matching requirements also indicate limits to the accessibility of binary salts as described in Table 2. While halides of all binary salts are commonly observed, the charge requirements imposed by the anions make the preparation of classic MN_3 salts virtually impossible. Similarly, the requirements of +6 cations restrict the MO_3 structures to a limited number of transition-metal compounds.

Table 2. Charge Limits for Simple AX_n Salts

	AX	AX_2	AX_3	AX_4	AX_5	AX_6
halides	+1/−1	+2/−1	+3/−1	+4/−1	+5/−1	+6/−1
chalcogenides	+2/−2	+4/−2	+6/−2	+8/−2		
pnictides	+3/−3	+6/−3				
tetrelides	+4/−4					

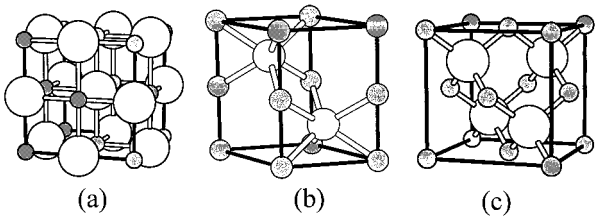

Figure 2. Structural variation of common AX salts. (a) NaCl structure-type, (b) NiAs structure-type, (c) ZnS structure-type. (*The cations are the small shaded spheres, while the large unshaded spheres are the anions. This convention will be used throughout the review.)*

Electron Configurations. *AX Salts.* While the charge matching synthetic strategy is frequently useful for the preparation of derivative structures of a given structure type, it in no way accounts for the structural variation of ions as a function of their electronic configuration. For example, while the halides NaCl, LaI, and CuCl, the chalcogenides MgO, ZrTe, and ZnS, and the pnictides ScN, NbSb, and GaN are, respectively, charge matched (based on a simple consideration of oxidation states), they represent three distinctly different structure types as shown in Figure 2. The sodium chloride structure is favored for the most ionic AX salts with an octahedral coordination exhibited by both anions and cations. The AX salts LaI, ZrTe, and NbSb, with formally d^2 electron configurations that favor metal−metal bonding, adopt the NiAs structure type in which the cation is coordinated in an octahedral environment of anions and the anions are coordinated to a trigonal prism of cations. The shared edges and faces of the octahedra are optimal for the formation of metal−metal bonds. Alternatively, AX salts which exhibit strong covalent bonding between anions and cations and utilize cations of main-group elements, or transition metals with a d^5 or d^{10} electron configuration, exhibit the sphalerite (zinc blende) structure in which both anion and cation are tetrahedrally coordinated. While

Table 3. ZnS (Zinc Blende, ccp) Structure Types

I/VII	II/VI	III/V
		BAs
		AlP, AlAs, AlSb
CuF, CuCl, γ-CuBr, γ-CuI	ZnS, ZnSe, ZnTe	GaP, GaAs, GaSb
γ-AgI	CdS, CdSe, CdTe	InP, InAs, InSb
	HgS, HgSe, HgTe	

each of these structure types is dictated by local bonding preferences of the constituent building blocks, the compilation of compounds in Tables 1 and 3 demonstrates that an opposing periodic relationship, resulting in isoelectronic materials with charge-matched cations and anions, can be articulated for both the ionic NaCl and covalent ZnS structure types.

Simple periodic trends are not easily tabulated for the NiAs structure type. A majority of NiAs structures are found for chalcogenides and pnictides,[18] while it has been observed for only one metal halide, LaI,[19] and a limited number of tetrelides. The added complexity of metal−metal bonding resulting from numerous structural instabilities further complicates this structure type.[20,21] A bonding description of metal−metal clustering distortions is not yet well articulated for the NiAs structure type (as, for example, has been described for the AX_2 salts below); nevertheless, such distortions demonstrate the importance of covalent and metallic bonding in this structure. At the same time, all of the first-row transition-metal selenides and a majority of the sulfides adopt this structure type in which M^{2+} cations are stabilized in the chalcogenide layers. This structural independence of the d-electron count argues for more ionic bonding models. In addition, both Ni and Pt are observed to adopt NiAs-type structures with group 13, 14, 15, and 16 anions.[18] Thus, while a systematic bonding picture of the NiAs structure will be rather complex, it is reasonable to predict that other halides and possibly more tetrelides may adopt this structure type.

AX_2 Salts. As described above for the AX salts, both charge and electron configuration are critical for the determination of the bonding, and thus the observed structure type, for AX_2 salts. Here, however, the electron count has more direct control over the observed structure types. The most ionic AX_2 salts, including all of the fluorides and a majority of the oxides, are observed to adopt either the fluorite or rutile structure types. A coordination number of eight in the fluorite structure type is preferred for the larger and more highly charged cations, whereas salts with smaller, lower charged cations adopt the rutile structure type. The first-row transition-metal oxides, and most of the transition-metal fluorides adopt the rutile structure, as opposed to the second- and third-row transition-metal oxides and rare-earth metal fluorides which adopt the fluorite structure.[13] The edge-shared octahedral chains of the rutile structure are well suited for distortions when metals are present with electron configurations favorable for metal−metal bonding. For example, MO_2 (M = Mo, W, Tc, V, Re, and Nb) all exhibit some form of dimerization along the edge-shared octahedral chains as a result of M−M bonding.[13] Similar distortions are less common for metal halides since the rutile structure is only observed for the first-row transition metals, which are less likely to form metal−metal bonds. Upon increasing the polarizability of the ions, the dichloride salts of the alkaline earth and several of the first-row transition metals adopt the layered, cubic closest packed $CdCl_2$ structure type.[9] This structure type is not known for any chalcogenide phases. A further increase in the polarizability of the constituent ions, thus increasing the covalent character of the M−X bonds, results in the formation of three-dimensional silicate-type structures when a coordination number of four is preferred and in the layered MoS_2, NbS_2, or CdI_2 structures for metals that prefer 6-fold coordination. In the latter, significant metal-atom clustering is observed for metals with electronic configurations suited for metal−metal bonding. By contrast, for the heavier chalcogenides, anion−anion bonding results in the formation of pyrite (FeS_2) structures. No pyrite structures are currently known for metal halides; however, framework structures formed with anion−anion bonding have recently been reported with polyiodide anions.[22]

Table 4. Cation/Anion Charge Matching for Silicate-Type Structures

$T^{6+}(X^{3-})_2$	"SN_2"	$[PN_2]^-$
$T^{4+}(X^{2-})_2$	SiO_2	$[AlO_2]^-$
$T^{2+}(X^{1-})_2$	$ZnCl_2$	$[CuCl_2]^-$
	BeF_2	

Silicate-Type Structures. Although fewer metals adopt a tetrahedral coordination geometry than an octahedral geometry, tetrahedral silicate-type structures dominate "inorganic natural products" composing 95% of the earth's crust.[23] Silicate structures are generally constructed from $SiO_{4/2}$ tetrahedra which are corner shared to other tetrahedral or octahedral building units. This construction motif is prone to extensive polymorphism with four crystalline phases present on the SiO_2 phase diagram in addition to many metastable and amorphous glassy phases.[16] Charge matching strategies for tetrahedral cation substitution have been extensively investigated in the large family of aluminosilicate materials since, as shown in Table 4, $[AlO_2]^-$ is isoelectronic and isostructural to SiO_2. As discussed for the AX salts, it is also possible to describe a related chemistry based on the opposing periodic trends of anion and cation substitution for these AX_2 salts. Substitution of N^{3-} for O^{2-} requires a concurrent move to the right on the periodic table for cation substitution from Si^{4+} to S^{6+} for charge balance. While SN_2 is not known to exist as a silicate-type structure, there are several known S_xN_y oligomers.[23] Nevertheless, the isoelectronic $[PN_2]^-$ has recently been discovered to adopt a structure analogous to high cristobalite in HPN_2[24] and $LiPN_2$.[25] Similar cristobalite-type structures are also observed for the isoelectronic $[SiPc_2]^{2-}$ and $[GePc_2]^{2-}$ (Pc = N, P, and As) building blocks.[26] By contrast, a move to the right on the periodic table upon anion substitution of F^- or Cl^- for O^{2-} requires a move to the left for cation substitution from Si^{4+} to Be^{2+} or Zn^{2+}. Both BeF_2 and $ZnCl_2$ are known to adopt cristobalite-type structures, demonstrate extensive polymorphism, and exhibit a rich chemistry of glass formation.[27−30] While no $[CuCl_2]^-$ has yet been shown to adopt a cristobalite-type structure, the cuprous chlorides also exhibit extensive polymorphism,[31] and as will be discussed below, copper zinc halides and lithium beryllium fluorides can be prepared to adopt structures analogous to aluminosilicates.

There are four crystallographically characterized phases of $ZnCl_2$,[32−35] but only α-$ZnCl_2$, which is iso-

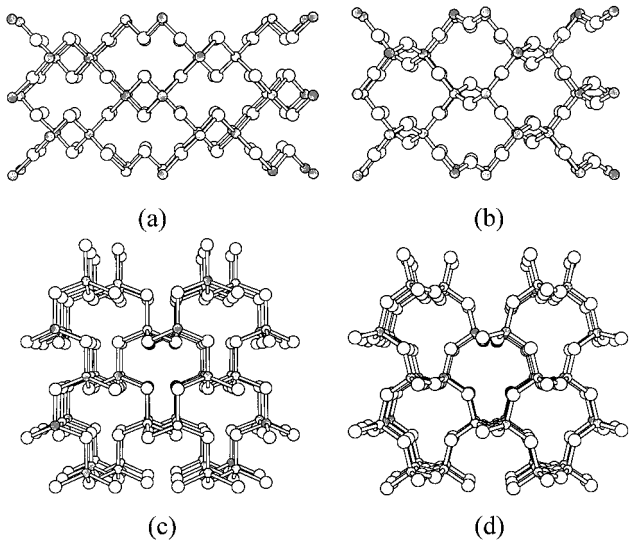

Figure 3. Ball and stick drawings indicating the similarity between the polymorphs of $ZnCl_2$ and SiO_2. (a) α-$ZnCl_2$, (b) high cristobalite, (c) δ-$ZnCl_2$, and (d) *Pna*2_1-cristobalite.

structural to high cristobalite (Figure 3), adopts a structure that is a direct analogue of SiO_2. The structure of δ-$ZnCl_2$ (or orthorhombic $ZnCl_2$) adopts an analogous structure to the *Pna*2_1-cristobalite structure observed for several ternary phases such as α-$NaGaO_2$.[36] δ-$ZnCl_2$ is the first binary compound of this structure type;[35] however, this structure has been predicted for SiO_2 by simulated annealing techniques.[37] A comparison of the oxide and chloride structures, as shown in Figure 3, clearly indicates that these AX_2 salts exhibit a common crystal structure (tetragonal, I-42d, and *Pna*2_1, respectively); however, the anions are ordered into layers in $ZnCl_2$, whereas in SiO_2 the anion layers are quite puckered. This is a result of the difference in the T−X−T bond angle (T = tetrahedral cation) dictated by the T−X bond distance. The longer Zn−Cl bonds, 2.31 Å, allow for a more acute T−X−T angle, 108.3°, without unfavorable T−T repulsions, than is possible for a silicate where the short Si−O bonds, 1.62 Å, favor the expanded Si−O−Si of approximately 140°. Both the BeF_2 (Be−F = 1.35−1.57 Å) and $[PN_2]^-$ (P−N = 1.65−1.72 Å) structures have metrical parameters much more similar to the silicates than to the zinc chlorides. This bond length influence on bond angles raises the possibility of framework flexibility resulting from a variation in the T−X−T angle. A maximal expansion to 180° gives the C9-diamondoid connectivity.[26] Interestingly, the contraction of the T−X−T angle to approximately 109° brings the anions into a closest packed arrangement in which the metal cations fill one-fourth of the tetrahedral holes. A (112) section of the α-$ZnCl_2$ structure contains the closest packed layers which are stacked in a cubic closest packed fashion. The δ-phase of $ZnCl_2$ contains the same closest packed layers but they are stacked in a hexagonal closest packed pattern. The limit to this T−X−T angle is imposed largely by the minimization of cation−cation repulsions. Thus, long T−X bonds will favor more acute T−X−T angles.

MX_2 Structures with Six Coordinate Cations. For the most part, metal dianions in which the cations prefer a coordination number of six and exhibit significant covalent bonding to the anions adopt a derivative of one of two layered structures with the metals in either a trigonal prismatic or an octahedral coordination geometry. Numerous polymorphs exist for the trigonal prismatic structures including 2H-MoS_2, 2H-NbS_2, 3R-MoS_2, and 3H-MoS_2. All of these contain the same MX_2 layers constructed of edge sharing trigonal prisms but differ in the stacking arrangement of the layers across the van der Waals gap. CdI_2 (1T-MX_2) is a derivative of a hexagonal closest packed lattice in which half of the octahedral holes are occupied such that van der Waals layers separate every other MX_2 layer of edge-sharing octahedra. It is not obvious what factors favor one structure over another as, for example, TaX_2 (X = S or Se) adopts both the 2H-MX_2 and 1T-MX_2 structures.[38−40] Nevertheless, both of these structure types exhibit a hexagonal lattice when undistorted but are susceptible to significant distortions driven by metal−metal bonding. The nature of the distortion has been described to be directly influenced by the d-electron count as well as the M−X bond distance.[41−43]

MoS_2- and NbS_2-Type Structures. The 2H-MX_2 layered structures and their stacking derivatives, which are composed of edge-sharing trigonal prisms, are most commonly observed for the Nb, Ta, Mo, and W chalcogenides. While the same extent of polymorphism is not yet known for the metal halides, $ZrCl_2$[44] with a d^2 electronic configuration adopts the 3R-MX_2 structure analogous to d^2 MoS_2[45] and WS_2.[46] Consistent with the band structure reported by Whangbo and Canadell,[42] the d^2 configuration fills the lowest d-block band, which is reasonably separated from other bands. The complete filling of this band favors the undistorted hexagonal lattice that is observed. By contrast, when this band is only half filled, as in salts with a d^1 electronic configuration, this hexagonal lattice is unstable with respect to distortion. In $NbSe_2$, TaS_2, and $TaSe_2$, a 3×3 super structure is observed at low temperature resulting from a metal atom trimerization caused by a charge density wave (CDW).[47−51] Halide analogues of a d^1-2H-MX_2 structure might be expected to be found among the lanthanide dihalides. In fact GdI_2 has been shown to adopt the 2H-NbS_2 structure.[52] While no low-temperature trimerization is reported for GdI_2, a ferromagnetic ordering is observed within the hexagonal layers below 313 K.[53] A weak trimerization would be consistent with this electronic localization. PrI_2 is also known to adopt both the 2H- and 3R-MoS_2 structures, again with no trimerization distortion reported. However, PrI_2 is also known to adopt numerous polymorphs including $CdCl_2$- and LaI_2-type structures as well as a unique $(PrI_2)_4$ cluster phase, which may be a result of the electronic instability of the d^1 configuration.[54] Alternatively, several lanthanide dihalides have been shown to add hydride to form LnX_2H_x (Ln = La, Ce, and Gd, X = Br and I)[55] in a similar fashion as TaS_2H_x,[56] to yield a 2H-NbS_2, 2H-MoS_2, or 3R-MoS_2 structure type. Here the hydride oxidizes the d^1 metal, depleting the lowest d-block band, resulting in semiconducting to insulating behavior upon increasing hydride content. This oxidation toward a d^0 configuration thus prevents the metal-atom clustering that results from a CDW-type instability.

CdI_2-Type Structures. The CdI_2 (1T-MX_2) and $CdCl_2$ structures can be considered stacking derivatives of layers composed of edge sharing octahedra. As noted

Table 5. Compounds with CdI_2, 1T-MX_2, Related Structures[a]

	halides			ref		chalcogonides			ref
d^0			CaI_2	76		TiS_2	$TiSe_2$	$TiTe_2$	77, 77, 77
						ZrS_2	$ZrSe_2$	$ZrTe_2$	78, 78, 79
						HfS_2	$HfSe_2$		13, 79
d^1			$LaI_2{}^T$	64			$VSe_2{}^{\sqrt{13}}$	$VTe_2{}^R$	60, 63
			NdI_2-II^T	65				$NbTe_2{}^R$	62
			PrI_2T	66		$TaS_2{}^{\sqrt{13}}$	$TaSe_2{}^{\sqrt{13}}$	$TaTe_2{}^R$	80, 81, 62
d^2	$TiCl_2{}^{Tr}$	$TiBr_2$	TiI_2	67, 82, 74	$LiVO_2{}^{Tr}$				68
			α-$ZrI_2{}^Z$	70		1T-$MoS_2{}^{Tr}$		β-$MoTe_2{}^Z$	69, 59
								$WTe_2{}^Z$	59
d^3	VCl_2	VBr_2	VI_2	73, 74, 74		$ReS_2{}^D$	$ReSe_2{}^D$		71, 72
d^4									
d^5		$MnBr_2$	MnI_2	83, 84				$CoTe_2$	85
								$RhTe_2$	86
d^6		$FeBr_2$	FeI_2	87, 88				$NiTe_2$	34
								$PdTe_2$	89
						PtS_2	$PtSe_2$	$PtTe_2$	89, 89, 89
d^7		$CoBr_2$	CoI_2	87, 88					
d^8	α-$PdCl_2{}^{JT}$			75					
d^9									
d^{10}			CdI_2	90					

[a] Superscripts: T, tetragonal distortion; $\sqrt{13}$, $\sqrt{13} \times \sqrt{13}$ super structure; Tr, trimerization; Z, zigzag chain; R, ribbon chain; D, diamond; JT, Jahn−Teller distorted chains.

above, the hexagonal closest packing observed in the CdI_2 structure type seems most favored for systems with significant covalent bonding between cation and anion. Thus, the $CdCl_2$ structure is infrequently observed for the heavier halides and not at all for the heavier chalcogenides. Like the trigonal prismatic layered structures, the electronic configuration of the metal is responsible for complex distortions of the ideal hexagonal lattice due to metal−metal bond formation described in Table 5. The band structure of the 1T-MX_2-type layer is significantly more complex than that of the corresponding 2H-MX_2-type layers.[42] The lowest three d-block bands exhibit considerable overlap consistent with the observation of the clustering distortions in materials with electron counts below d^6. Ideal hexagonal lattices (Figure 4a) are most commonly observed for materials with d^0, d^6, and d^{10} electron configurations and for higher temperature phases of materials with intermediate electron counts. However, MX_2 salts capable of metal−metal bonding exhibit a variety of structural distortions upon partial filling of these metal−metal bonding bands as described in Table 5. It has been noted that among metals with a given d-electron configuration weak distortions are typically observed for compounds with short M−X bonds, whereas systems with longer M−X bonds generally involve a stronger distortion as seen for $LiVO_2$[57,58] vs WTe_2.[59]

d^1. To date, only the chalcogenides are known to adopt truly d^1 1T-MX_2-type structures. The partial filling of the lowest two d-block bands results in an electronic instability such as the observed $\sqrt{13} \times \sqrt{13}$ clustering of metals observed for VSe_2.[60] In fact, some degree of structural tunability has been observed for the mixed-metal ditelurides.[43] This clustering does not expressly correspond to Fermi surface nesting but is considered to originate from local chemical bonding. Related $\sqrt{4} \times \sqrt{4}$, and $\sqrt{7} \times \sqrt{7}$ clustering have been reported for VSe_2 and $\sqrt{19} \times \sqrt{19}$ clustering in $NbTe_2$.[61] A ribbon-type distortion which corresponds to a trimerization along the a and $(a + b)$ lattice directions is observed for MTe_2 (M = V, Nb, or Ta).[62,63] This is a result of a common nesting vector associated with two one-third filled bands of a $d^{4/3}$ electron configuration. This ribbon chain is observed only for the tellurides in which significant occupation of Te−Te bands is observed, such that the oxidation state of Te is reduced from the formal oxidation state of Te^{2-}. No metal halides exhibit these types of electronic distortions. However, LaI_2, NdI_2, and PrI_2 adopt a similar layered structure[64−66] which exhibits a tetragonal distortion shown in Figure 5. This tetragonal distortion places the lanthanide in the center of an iodide cube. In fact, the relationship between the CdI_2 structure and the LaI_2

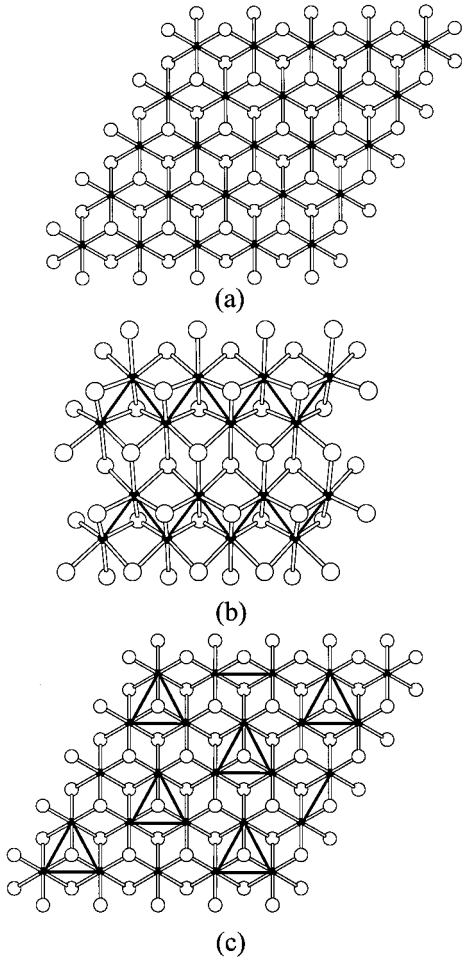

Figure 4. Ball and stick representation of the ideal hexagonal lattice found in a (a) CdI_2 layer viewed down the *c* direction and (b) the zigzag chain and (c) trimerization distortions caused by a CDW instability.

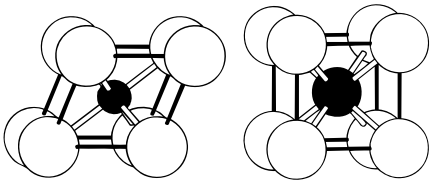

Figure 5. View of the hexagonal and tetragonal cells of (a) CdI_2 and (b) LaI_2, respectively, illustrating that the relationship between the two structure types is analogous to the relationship between the NaCl and CsCl cells.

structure, where the octahedral or cubic holes, respectively, of every other anion layer are occupied, is exactly analogous to the relationship between NaCl and CsCl. The large lanthanide cations do not readily fit into the smaller octahedral holes of a 1T-MX_2 lattice and thus distort the structure to a tetragonal lattice. While no specific M−M bonding distortions are reported for these LnX_2 materials, the bonding has frequently been described as a $Ln^{3+}(e^-)(I^-)_2$ in which the $5d^1$ electron is delocalized in a conduction band consistent with the observed metallic properties. The existence of several other structure types for other lanthanide dihalides may in fact be related to the instability of the d^1 configuration with respect to metal−metal bonding distortions,[7] but a more in-depth structural study would be required to articulate such relationships.

d^2. Two structural distortions of the 1T-MX_2 lattice are observed for compounds with the d^2 electron configuration as shown in Figure 4b,c. Whereas $TiCl_2$, 1T-MoS_2, and $LiVO_2$ exhibit a trimerization,[67−69] α-ZrI_2, *β*-$MoTe_2$, and WTe_2 exhibit the formation of zigzag chains.[59,70] The electronic band structure of the nondistorted layer can be figuratively described as the superposition of three "hidden 1-D bands" from the one-dimensional chains of edge-sharing octahedra.[42] The two d-electrons can thus fill either one-third of all three of the bands, which gives rise to a 3×3 superstructure consistent with the trimerization, or fill half of two bands, resulting in a dimerization along two of the three chain directions consistent with the observed zigzag chain. For the isoelectronic halides and chalcogenides, a trimerization is observed for systems with the shortest M−X bonds, whereas zigzag chains are observed when longer M−X bonds are present. The compounds with shorter M−X bonds also exhibit shorter metal−metal contacts and thus a greater dispersion of the d-block bands. As the bandwidth increases, the disproportionate band filling of the zigzag chain becomes much less favored with respect to the delocalized trimer because of a greater promotional energy for reorganization. Conversely, the longer M−M and M−X bonds are not sufficiently stabilized by the delocalized three-center bonding of the metal trimer. As a consequence, localized two-center two-electron bonding is observed forming a zigzag chain.

d^3. The bonding in d^3 1T-MX_2 can similarly be understood from the principles of electronic structure described for the d^2 phases in which each of three hidden 1-D bands is half-filled. The resulting diamond clustering observed for ReX_2 (X = S, Se)[71,72] can equally be described as a CDW instability derived from two nesting vectors or as the formation of three localized two-center, two-electron bonds. A more symmetrical distortion derived from three nesting vectors might be expected for an oxide structure with shorter M−X bonds. No distortions are reported for the structures of the VX_2 (X = Cl, Br, I)[73,74] salts, nevertheless, it would be interesting to examine the low-temperature behavior of these phases.

d^4. MX_2 phases with a d^4 electron count are notably absent from both halide and chalcogenide materials. In the metal halide systems, for example, while $CrCl_2$ adopts a distorted rutile structure, both Mo and W form cluster phases such as W_6X_{12}.[13] Clearly, metal−metal bonding dominates the phase formation causing major clustering as described below. By contrast, the formally d^4-chalcogenide FeS_2 adopts the pyrite structure where X−X bonding reduces the oxidation of the metal such that it is better described as d^6. As noted above, the pyrite structure has not been observed for any halide materials; however, similar bonding is observed for a variety of pnictides, yielding, for example, the isoelectronic and isostructural FeS_2 and *β*-$NiAs_2$.

d^8. A d^8 electronic configuration in an octahedral geometry is expected to be unstable with respect to a Jahn−Teller distortion. A distortion which lengthens two M−X bonds in a 1T-MX_2 layer will break the three hidden 1-D edge-shared octahedral chains into one set of edge-shared square-planar chains as observed for α-$PdCl_2$.[75] No d^8 transition-metal chalcogenide phases exist since no d^8 M^{+4} ion is known. Instead, for example CdS_2 adopts a pyrite structure with Cd^{2+}.

AX_3 Salts. A rich structural variation is observed for metal-halide AX_3 salts including molecular and one-, two-, and three-dimensional species as recently reviewed by Lin and Miller.[3] Like the AX_2 salts, this complex structural variation is significantly influenced by metal−metal bonding distortions as a function of their d-electron count. A similarly diverse chemistry cannot be observed, however, for chalcogenide analogues since the AX_3 stoichiometry requires cations with a +6 charge, thus limiting possible cations to transition metals later than group six. In fact, transition-metal trioxides are only known for Cr, Mo, W, and Re. For the heavier chalcogenides only $CrTe_3$, $NbSe_3$, and TaS_3 are found from a search of the Inorganic Crystal Structure Database. $NbSe_3$ and TaS_3 have an unusual valence though, in which the chalcogenide does not have a −2 charge. The compositional diversity is reversed in ABX_3 salts, with chalcogenides exhibiting a greater range of composition than halides. Such halide salts are restricted to combinations of +1 and +2 cations to balance the −3 charge of the anions, whereas +1/+5, +2/+4, and +3/+3 combinations of cations will charge balance the −6 charge of chalcogenide anions. A rich structural chemistry resulting from complex patterns of metal−metal bonding is similarly observed for chalcogenide ABX_{3-x} materials, which exhibit d-electron counts between d^0 and d^4.[91] Structural relationships between more complex halides and oxides will be discussed later.

Summary of Construction Principles. The above analysis of simple AX_n salts reiterates several principles of bonding that can be exploited for the construction of metal halides with the structure types of known chalcogenides, while also noting expected boundaries where these analogies must break down. (1) In the ionic

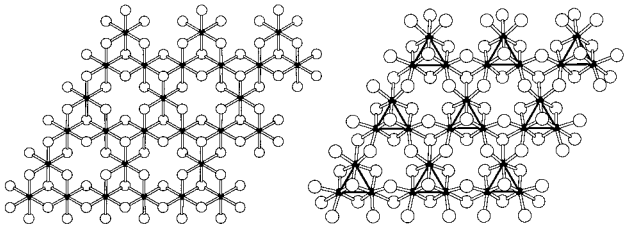

Figure 6. (a) Ball and stick drawing of an undistorted M_3X_8 layer viewed down the *c* axis. (b) Trimerization of the M_3X_8 layers found in $Zn_2Mo_3O_8$ and the low-temperature structure of $Na_2Ti_3Cl_8$.

bonding limit, the size and charge of ions are the dominant influences that determine the structure of solids. These size and charge arguments are also important in the construction of covalent solids. (2) As the A−X bonds become more covalent, the geometric preferences of the cation become heavily influenced by its electron configuration such that local octahedral, tetrahedral, square planar, etc. geometries are observed. (3) Heavier element combinations add the possibilities of A−A interactions, seen in a rich variation of metal−metal bonding. X−X interactions, on the other hand, may also become significant, particularly in the case of the heavier chalcogenides and pnictides. (4) The A−X bond distances have a major impact on the A−A contacts such that short A−X bonds will require long A−A distances in cases of A- -A repulsion or will favor short A−A contacts when metal−metal bonding is viable.

Construction of Complex Halide/Chalcogenide Analogues

In the second half of this review, these principles are shown to be important to understanding the relationship between halides and chalcogenides of selected complex structure types, and we demonstrate the utilization of such principles for the construction of new metal-halide materials derived from known chalcogenide analogues.

Metal-Atom Clustering in Complex Structure Types. *$M_3X_8^{n-}$.* Intermediate in structure and composition between a 1T-MX_2-type and a BiI_3-type layered structure are a series of solids which contain $M_3X_8^{n-}$ layers. The edge sharing octahedra which make up this layered structure are well suited for metal−metal bonding, depending on the metal d-electron count. In the nondistorted structure, shown in Figure 6a, six MX_6 octahedra share edges to form a regular hexagon with an "empty X_6 octahedron" in the center. The ideal lattice is observed in the structure of $Na_2Mn_3Cl_8$[92] in which the high-spin d^5-electron configuration is not susceptible to a distortion from octahedral symmetry. By contrast with a d^2-electron configuration, both $[Mo_3O_8]^{4-}$ [93] and $[Ti_3Cl_8]^{2-}$ [94] exhibit a trimerization of their crystal structure (Figure 6b) at or below room temperature, respectively, analogous to the metal−metal bond driven distortion in the d^2-1T-MX_2 compounds previously described. Substitution of the Mo by V requires an increase in the charge on the layers by −3 as observed for the $[V_3O_8]^{7-}$ layers within NaV_6O_{11}.[95] With an identical electron configuration, the $[V_3O_8]^{7-}$ layer in sodium vanadate undergoes a similar trimerization at low temperature.

$(M_6X_8)X_6^{n-}$ and $(M_6X_{12})X_6^{n-}$ Clusters. An examination of the simple binary MX_2 and MX_3 salts finds no simple halide or chalcogenide salts with a d^4 electron configuration other than CrX_2 (X = Cl, Br), which adopts the distorted rutile structure as noted above. Rather, salts with d-electron counts between d^3 and d^4 are unstable with respect to the formation of metal−metal bonded clusters. Homoleptic d^3 metal halides of the second- and third-row transition metals with the MX_2 and MX_3 stoichiometry form cluster phases such as Ta_6Cl_{12} and W_6Cl_{18},[96] respectively, whereas d^4 metal halides of the same compositions form Mo_6Cl_{12}[97] and Re_3Cl_9[98] clusters, respectively. By contrast, no homoleptic d^3 or d^4 MX_3 chalcogenide phases exist, and the d^3 MX_2 chalcogenides exhibit a metal−metal bond driven diamond chain-type clustering described above. Nevertheless, slight compositional variations in the M/X ratio for both halides and chalcogenides and/or the inclusion of interstitial atoms or extracluster cations while maintaining a d-electron count of between $d^{2.5}$ and d^4 results in the formation of a large variety of octahedral cluster phases as summarized in Table 6. Only selected cluster phases are reported here to highlight the relationship between the halides and chalcogenides, since numerous reviews discuss such cluster phases.[99−104]

Two basic cluster units are observed consisting of either an M_6X_8 core in which the ligands cap the faces of the octahedral cluster, or with an M_6X_{12} core where the ligands bridge the edges of the cluster (Figure 7).[99−104] In both cases, these bridging ligands are designated as inner ligands, X^i. Six terminal ligands attach to each type of cluster in apical positions and are designated as outer ligands, X^a. The observed compositional range from M_6X_{18} to M_6X_8 is a reflection of the extent of condensation of cluster connectivity through anion bridges. For example, a structure in which all six of the terminal ligands are shared between two neighboring clusters would be represented as $(M_6X^i_{12})X^a_{6/2}$ or M_6X_{15}. Several of these reports have discussed the bonding requirements of these octahedral clusters and found that the M_6X_8-type geometry is most favorable for clusters with 24 cluster bonding electrons (d^4 per metal), whereas the M_6X_{12}-type geometry is favored for the less electron rich clusters with an optimal 14 or 16 cluster bonding electrons ($d^{\sim 2.5}$ per metal). In these phases, when the number of cluster bonding electrons is insufficient for the preferred cluster bonding additional electrons are obtained either via interstitial stabilization to yield $(M_6Z)X_{12}$ cores or via the addition of extracluster cations. Alternatively, mixed halide/chalcogenide clusters allow further compositional variation of a given structure type. Thus a fine-tuning of the metal, the number and charge of the anions, and the presence of interstitial or extraframework cations can be exploited for the construction of an extensive family of cluster phases. Similar bonding analogies can be drawn between a variety of halide and chalcogenide condensed cluster phases, such as the relationship between the interstitially stabilized Sc_4Cl_6B[105] and the extraframework cation stabilized $NaMo_4O_6$.[106]

Tetrahedral Structure Types. Having observed the structural relationships between halide and chal-

Table 6. Metal Halide and Chalcogenide M_6X_8 and M_6X_{12}-Type Clusters

	$(M_6X_8)X_6$				$(M_6X_{12})X_6$			
	halide	ref	chalcogenide	ref	halide	ref	chalcogenide	ref
M_6X_{18}					W_6Cl_{18}	96	$Nb_6Cl_{13}O_3^{5-}$	107
M_6X_{17}								
M_6X_{16}					$Zr_6Cl_{16}B^{3-}$	99	$Nb_6Cl_{13}O_3^{3-}$	108
M_6X_{15}					Ta_6Cl_{15}	109		
M_6X_{14}	$Mo_6Cl_{14}^{2-}$	110	$Co_6Se_8(PPh_3)_6$	111	Nb_6Cl_{14}	112		
M_6X_{13}	$Mo_6Cl_{13}^{-}$	113			$Zr_6Cl_{13}B$	99		
M_6X_{12}	Mo_6Cl_{12}	114	$Re_6S_{12}^{4-}$	115	$Zr_6Cl_{12}Be$	99	Nb_6O_{12}	
M_6X_{11}	Nb_6I_{11}	116	$Re_6S_{11}^{4-}$	117	$Sc_6I_{11}C_2$	118	$Nb_6O_{11}^{6-}$	119
M_6X_{10}	$Mo_6Br_8S_2$	120	$Re_6Se_8Cl_2$	121	$Y_6I_{10}Ru$	122	$Mo_6O_{10}^{2-}$	123
M_6X_9	$[HNb_6I_8]I_3$	124						
M_6X_8	$Nb_6I_8^{2+}$		Mo_6S_8	125				

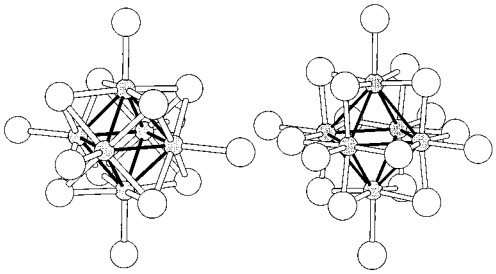

Figure 7. Ball and stick drawings of the (a) $(M_6X^i_8)X^a_6$ and (b) $(M_6X^i_{12})X^a_6$ clusters.

cogenide phases which exhibit extensive metal−metal bonding, it was interesting for us to attempt to exploit similar bonding principles for the construction of analogues of a radically different class of materials such as silicates and phosphates. Such materials are influenced primarily by the local geometry of the building blocks as opposed to the propensity to form metal−metal bonds.

Complex Silicate-Type Structures. Starting from the observed relationship between $ZnCl_2$ and SiO_2, we set out to prepare metal-halide structural analogues to aluminophosphate and aluminosilicate zeolitic materials.[11] Although these metal-halide materials will not yield refractory microporous framework materials such as are typically used for hydrocarbon processing, new chemical transformations are expected to be viable if we can engineer Lewis acidic and redox active metal-halide building blocks into crystalline frameworks which exhibit size and shape selectivity. To achieve our goal of metal-halide zeotype-framework design, we must (1) utilize $MX_{4/n}$-type building blocks for which a tetrahedral coordination is favored by the metal's d-electron count, (2) exploit the principles of charge matching, (3) control the relative size of framework and templating ions, and (4) be attuned to structural effects dictated by variation in M−X bond distances.

$MM'X_4$. Charge matching principles, analogous to those relating SiO_2 and $AlPO_4$, should in principle be paralleled by a relationship between $ZnCl_2$ and $CuMX_4$ (M = Al, Ga; X = Cl, Br, I).[126] A direct analogue of the α-$ZnCl_2$[32] structure type is found in the structure of $CuGaI_4$.[127] Here, the $CuI_{4/2}$ tetrahedra (Cu−I = 2.62 Å) and the $GaI_{4/2}$ tetrahedra (Ga−I = 2.56 Å) are virtually of identical size and thus the +1 and +3 cations directly substitute for two Zn^{II} cations. However, in $CuAlCl_4$ the $CuCl_{4/2}$ tetrahedra are significantly larger (Cu−Cl = 2.36 Å) than the $AlCl_{4/2}$ tetrahedra (Al−Cl = 2.14 Å). The difference in size of the tetrahedral building blocks of $CuMX_4$ (M = Al, Ga X = Cl, Br) results in a doubling of the unit cell. Like $ZnCl_2$, the atom arrangement in $CuMX_4$ structures can be described as the stacking of closest packed layers in a cubic closest packed fashion to yield the tetragonal α-$CuMX_4$[126,128,129] or a hexagonal closest packed fashion to yield the orthorhombic β-$CuMX_4$,[126] as shown in Figure 8. The β-phase of $CuMX_4$ has been shown to be metastable with respect to the α-phase and can only be synthesized by rapid quenching from a melt.

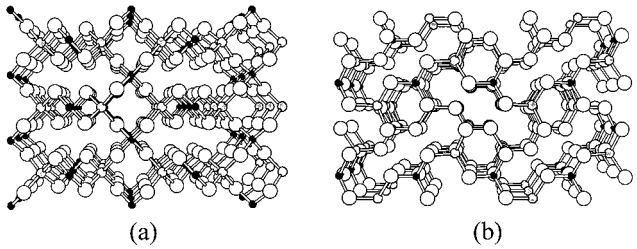

Figure 8. Ball and stick representations of (a) α-$CuAlCl_4$ looking down *a* and (b) β-$CuAlCl_4$ looking down *c*. The smaller shaded spheres are Al and the larger shaded spheres are Cu.

The cations of both $ZnCl_2$ and $CuMX_4$ order into zigzag chains, occupying only one-fourth of the tetrahedral holes of the approximately closest packed anion sublattice. The ordering of the vacant holes in the lattice creates notable "van der Waals" channels throughout the framework. These channels are physically too small for penetration by small molecules (for $CuAlCl_4$ the cross-channel Cl−Cl contacts being 0.2−0.4 Å greater than the sum of the van der Waals radii of Cl). Nevertheless, we have shown by gravimetric analysis, spectroscopy, and real time powder diffraction that α-$CuAlCl_4$ can reversibly chemisorb 0.5−1.0 molar equiv of small molecule gases such as C_2H_4, CO, and NO. This gas sorption may also be related to the reversible benzene adduct formation of $(C_6H_6)CuAlCl_4$,[130] although different adduct structures are observed for different adduct molecules.[131] A common adduct is observed upon sorption from either the α- or β-phase, but upon gas desorption only the thermodynamically favored α-phase is observed. In the case of the ethylene adsorption into α-$CuAlCl_4$, at least one intermediate phase is observed by real time powder diffraction.[132] The X-ray powder diffraction of the final ethylene adduct confirms that a tetragonal phase with lattice constants of $a = b = 6.33$ and $c = 12.38$ Å is formed. This powder pattern is consistent with a model in which the framework is expanded at the M−Cl−M′ angles from 109° to 180°, yielding a $[NMe_4][CuPt(CN)_4]$-type structure[133] in which the olefins are coordinated to an opened coordination site on one of the metals. This flexibility of the T−X−T angle is along a similar distortion coordinate that

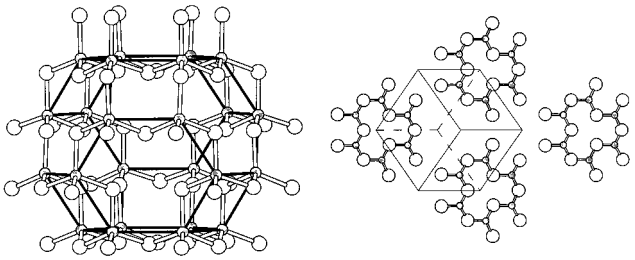

Figure 9. Ball and stick representation of the sodalite cage found in (a) $[HNMe_3][CuZn_5Cl_{12}]$, CZX-1, and (b) a (111) section emphasizing in the ccp anion sublattice with $^4/_{16}$ of the anion sites vacant.

relates α-$ZnCl_2$ to high-cristobalite (see above) and results in >3 Å channels. While various structures are formed by the small molecule adsorption into the $CuAlCl_4$ framework, in all cases, the reversible sorption process appears to be dictated in part by the flexibility of the metal-halide frameworks.

$[M_nM'_{m-n}X_{2m}]^{n-}$. Aluminosilicates, which include the diverse family of zeolites, exploit the principles of charge matching to create open framework structures. A charge deficient tetrahedral cation is substituted for certain of the Si^{4+} framework cations in order to create an anionic lattice, and extraframework cations balance the charge of the framework as well as serve to fill space and/or template the framework construction. By analogy, it should be possible to substitute charge deficient cations into the zinc chloride lattice for similar halozeotype constructions. This is observed by replacing certain Zn^{2+} framework cations with Cu^+ in $ZnCl_2$ to yield $[Cu_nZn_{m-n}Cl_{2m}]^{n-}$ that must be charge balanced and templated by extraframework cations.

The Sodalite Structure. Trimethylammonium cations serve to template the formation of β-cages resulting in the sodalite structure, $[HNMe_3][CuZn_5Cl_{12}]$, CZX-1, shown in Figure 9a.[11] (CZX is defined as the common name for this family of copper zinc halides.) Using the geometric constraints described for oxide-based sodalite, a cubic lattice constant of 10.55 Å is predicted for a sodalite cage constructed out of ideal tetrahedra (α = 109.4°) with a M−X bond distance of 2.28 Å and a T−X−T angle of 109.4° (φ = 45°).[134] Crystallizing in the cubic space group *I*$\bar{4}$*3m*, with **a** = 10.5887(3) Å, CZX-1 very nearly exhibits the ideal structure for a contracted β-cage. Geometrically, the T−X−T angle can vary from 109.4° to 160° according to the extent of cage expansion. The observed T−X−T angle of 110.04(3)° in CZX-1 is markedly more contracted than any known oxide based sodalite where the T−O−T angles range from 124 to 160°.[135] The minimum angle is limited by the T−X bond distances which determine the T−T separations. Despite this most contracted cage, the larger T−X bond distance in the metal halide framework still yields a sodalite cage with the largest known cell volume.

The structural comparison between the oxide- and halide-based sodalite structures is parallel to that described above for $ZnCl_2$ and SiO_2 and is similarly evident in the respective anion arrangements. With a nearly ideal tetrahedral angle at Cl, the halide-based sodalite structure clearly shows a cubic closest packing arrangement of the framework anions. The role of the template is to fill $^4/_{16}$ of the closest packed anion sites such that the β-cages could be formed (Figure 9b). Constructions with larger templating cations and/or the inclusion of solvent are anticipated to yield expanded cages with T−X−T angles in the range of that observed for oxide-based materials.

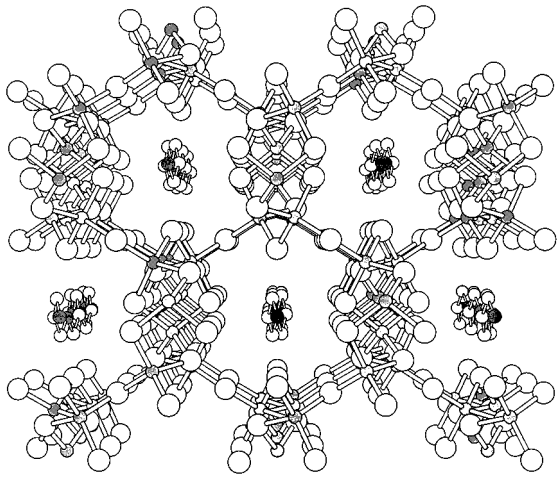

Figure 10. Ball and stick representation of $[H_2NEt_2][CuZn_5Cl_{12}]$, CZX-2, viewed along the *a* direction, which shows the position of the templating cation within the 11-ring channel.

A Novel Microporous Framework. Syntheses utilizing the more rodlike diethyl- or dimethylammonium cations result in the templated growth of a novel zeotypic framework with a three-dimensional channel structure shown in Figure 10.[11] CZX-2, $[H_2NEt_2][CuZn_5Cl_{12}]$, and CZX-3, $[H_2NMe_2]_n[Cu_nZn_{6-n}Cl_{12}]$ (n = 1 or 2), consistent with our aluminosilicate analogy, are also constructed from corner sharing tetrahedral primary building units. Like the halozeotype described above, these materials also exhibit T−X−T angles of 110°, which is well contracted below that observed for any aluminosilicates. Nevertheless, the connectivity of this framework cannot be described from a closest packing of anions. Unlike the sodalite cage, this structure is not geometrically flexible, since an opening of the T−X−T angles also requires significant distortion to the $MX_{4/2}$ tetrahedra. For this reason, the CZX-2 structure type is only expected to be observed for frameworks constructed from building blocks with long T−X distances.

The most open direction of the CZX-2 framework consists of channels running along the 2_1 axes parallel to *b*. The smallest ring to circumscribe this channel consists of 11 tetrahedra. As shown in Figure 10 (for CZX-2), the templating dialkylammonium cations reside in the center of these channels and are hydrogen bonded to the chloride channel interior. In the stuffed n = 2 CZX-3, the dimethylammonium cations are oriented in a slightly different fashion within the same channels in order to maximize hydrogen bonding. The shortest cross-channel contacts are 6.34 Å for CZX-2, which corresponds to a free diameter of 2.9 Å given the van der Waals radii of Cl = 1.7 Å. These are smaller openings than traditionally observed for an 11-ring since the T−X−T angle of 110° results in a collapsing of the window. Four eight-ring windows provide entry into the primary 11-ring channels forming smaller channels along the body diagonal. The largest void in the fully occupied CZX-3 structure is centered directly in the eight-ring window and also corresponds to the channel parallel to the *c* axis with the shortest void-centroid-

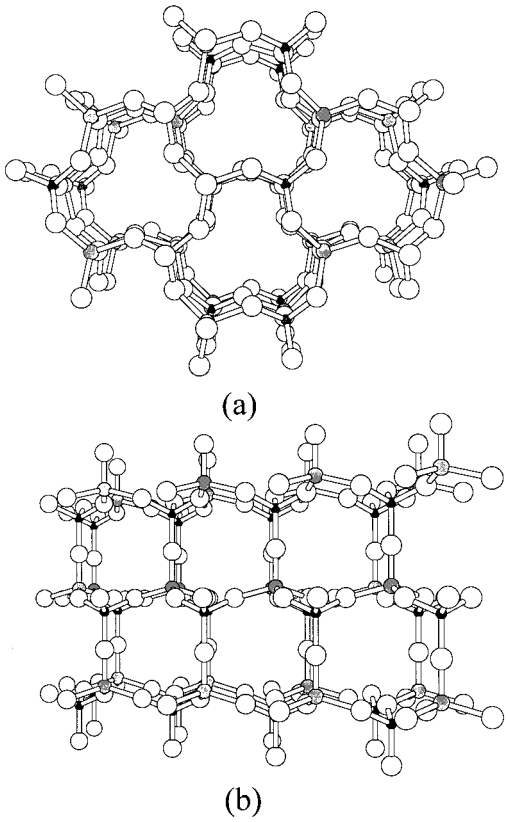

Figure 11. Ball and stick representations of the anionic sublattices (a) $CsLiBeF_4$ viewed along the *c* direction and (b) $KLiBeF_4$ viewed along the *b* direction. The smaller shaded spheres are Be and the larger shaded spheres are Li.

to-halide distance of 2.69 Å. This void space, in addition to the void created by template vacancy in CZX-3 (n = 1), is of appropriate size to adsorb small molecules such as methanol. While this solvent adsorption also results in colloid formation, we have shown that CZX-3 (n = 1) adsorbs 1.8 mol per formula unit more methanol than does its stuffed n = 2 counterpart.

Lithium Beryllium Fluoride Frameworks. A similar analogy between oxide and halide frameworks is observed starting from a BeF_2 parentage. As noted above, BeF_2, $ZnCl_2$, and SiO_2 exhibit common structural motifs and all can be readily supercooled to glassy phases.[29,30] Since Li^+ readily adopts a tetrahedral coordination geometry, charge matching strategies by which certain Be^{2+} sites are substituted by Li^+ to yield an anionic framework can be exploited to create a family of $[A]_n[Li_nBe_{m-n}F_{2m}]$ materials. In fact, a survey of the Inorganic Crystal Structure Database finds four three-dimensional lithium beryllium fluorides, two of which are direct analogues of aluminosilicate structure types. Bu and Stucky recently pointed out that both $[N_2H_5]^+$ and $[Cs]^+$ template the formation of an ABW-type zeolite framework with eight-ring channels running along *b* and *c*.[136−138] (The latter is shown in Figure 11a.) Similarly the three-dimensional framework $[K]LiBeF_4$[139] is isostructural to $[K]AlSiO_4$[140] in which channels of six-rings penetrate the lattice along *a*, *b*, and *c*, the former being shown in Figure 11b.

Unlike the CZX materials, these LiBeF materials exhibit metrical parameters much more similar to those of the silicates with Be−F = 1.55 Å and Li−F = 1.85 Å, as compared with Si−O = 1.62 Å and Al−O = 1.73 Å.

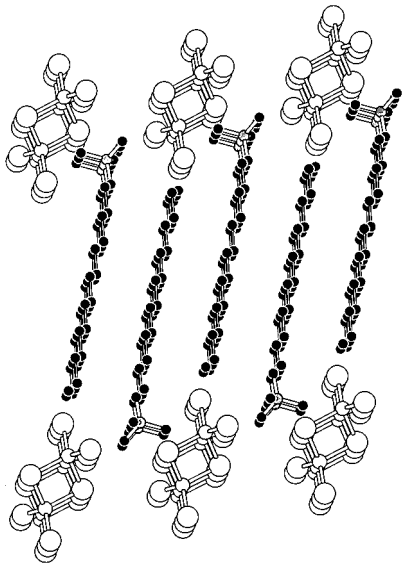

Figure 12. Ball and stick representation of $[CTA]_2Zn_2Cl_6$, MZX-1, viewed along the *a* direction.

Thus, as observed for all oxide structures, the short metal−fluoride bond distance will require a more obtuse T−X−T angle. The elongated Li−F distance, with respect to the Al−O distances, results in a slightly contracted T−X−T angle, observed to be on the order of 130° in several $[LiBeF_4]^-$ crystal structures. Nevertheless, the closest packed-type geometry observed for the metal chlorides is not expected to be observed for the fluorides.

Surfactants as Templates. Upon successful demonstration of the concept of the construction of metal-halide analogues to zeolites, we have begun to explore the limits of such framework construction by attempting to prepare metal-halide analogues of mesostructured materials in the M41S family.[141,142] We do not expect the halide frameworks to be stable upon the removal of the templating surfactant; however, the softer metal-halide lattice may facilitate crystal growth that will provide useful structural models for the silicate analogues. A family of MZX (mesostructured zinc halides) can readily be prepared from CTAB (cetyltrimethylammonium bromide) and $ZnCl_2$.[143] Single crystals of MZX-1, $[CTA]_2Zn_2Cl_6$, were grown from methanol solutions of a 1:1 mixture of the starting materials. MZX-1 (Figure 12) adopts a lamellar structure with a basal spacing of 14.9 Å, which is significantly less than the length of the CTA surfactant as a result of a canting of the alkyl chains with respect to the stacking planes. The anionic inorganic spacers, $Zn_2Cl_6^{2-}$, edge shared tetrahedral dimers, are associated with the cationic headgroups of the detergent. This metal-halide structure is a cation deficient analogue of the previously characterized chalcogenide, $[C_{12}TA]_4Sn_2S_6{\cdot}2H_2O$ ($C_{12}TA$ = dodecyltrimethylammonium).[144] The canting of the C_{16} cation chains in cation deficient MZX-1 results in nearly identical lattice constants to the tin sulfide lamellar phase with twice the number of shorter, C_{12}, cations. Increasing the surfactant to $ZnCl_2$ ratio to 2:1 results in the formation of a new lamellar phase, MZX-2, with an increased basal plane separation of 31.6 Å as determined from the orthorhombic cell of a = 7.82 Å, b = 31.56 Å, and c = 5.21 Å. The indexed diffraction pattern of MZX-2 is shown in Figure 13. The structure

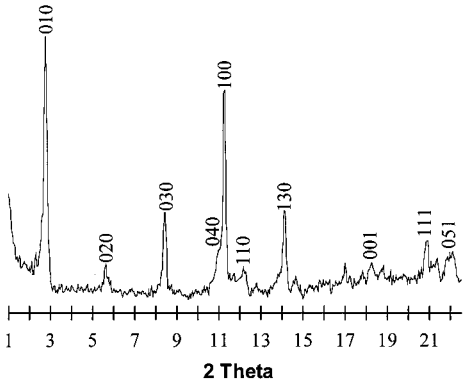

Figure 13. Powder X-ray diffraction pattern for MZX-2.

of MZX-2 is expected to be analogous to the lamellar $[H_3N(C_nH_{2n+1})]_2ZnCl_4$ structures.[145] In addition to directing structure formation, the surfactant/$ZnCl_2$ ratio also can be exploited to direct liquid crystalline formation. The liquid crystalline properties of these MZX materials will be described in a future work.[143] We anticipate that control of the liquid crystalline phases will be important for the directed synthesis of hexagonal mesostructured phases.

Non-Silicate Tetrahedral Structures. As described above, silicate structures are rather restricted in their local structural organization due to the short Si−O bonds with respect to the size of the silicon cations. By contrast, metal−chloride distances are long with respect to the size of transition-metal cations. Thus, while several of the above structure types demonstrate analogy to silicates, a greater commonality may be anticipated for oxides of smaller cations such as borates, or for main-group sulfides.

AM_4X_7. The $M_4X_7^{n-}$-type frameworks exhibit a variety of structural connectivities in order to accommodate the local bonding requirements of the respective building units. Deviating from the traditional MX_2 corner-sharing tetrahedral structural motif, in which all anions are two coordinate, the $M_4X_7^{n-}$ stoichiometry requires a variation in framework connectivity such as three coordination at certain anions ($BaAl_4S_7$),[146] edge sharing tetrahedral connectivity (HP_4N_7),[24] and/or a combination of octahedral and tetrahedral local geometries ($SrAl_4O_7$).[146] It is the $BaAl_4S_7$ structure type that is exhibited by the frameworks for which the M−X bonds are long with respect to the size of M and thus is the observed structure for $[A]Cu_2Zn_2Cl_7$, A = H_3NMe and Cs (CZX-4 Figure 14). Interestingly, $[Cs]Li_2Be_2F_4$[136] also adopts this structure type although it is not known for any aluminosilicate phases. The structure of this framework is most readily described from a closest packing morphology in which one-eighth of the anion sites of a closest packed layer are occupied by the extraframework templating cations.[147] These layers are then stacked in a hexagonal closest packed fashion such that each template resides in a cage of 12 anions. This closest packed type structure is observed when the T−X−T bond angle can approach an ideal tetrahedral angle of 109.4°. This structure is found as the resultant phase when templating the copper zinc halides with either H_3NMe^+ or Rb^+ to yield CZX-4. Consistent with the longer M−X bonding, this structure type is identical to the known BaM_4S_7 (M = Al, Ga),[148] in which one of the anions is three coordinated. Because of the local geometric constraints imposed by short metal-oxide distances, $B_4O_7^{2-}$ is the only oxide framework with this structure type since B^{3+} is a very small cation.[149] Yet even here, the short B−O bond distance requires a significant expansion of the T−X−T angle to a range of 115−140°. Completely different polyhedral connectivities are required in the structure of aluminates and gallates, which favor T−X−T angles of approximately 140°. The slightly longer distances of the lithium and beryllium tetrahedra, which favor T−X−T angles of approximately 130°, allow this structure type to be adopted by $RbLi_2Be_2F_4$. However, its structure is significantly distorted away from the ideal closest packed-type geometry.

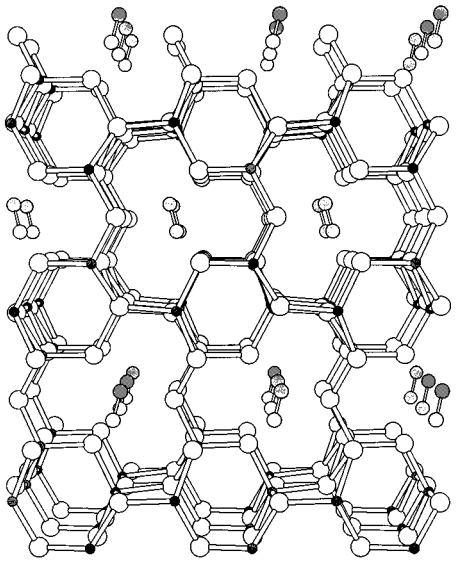

Figure 14. Ball and stick representation of $[H_3NMe][Cu_2Zn_2Cl_7]$, CZX-4.

Frameworks from Condensed Tetrahedra. Another type of framework observed for species with more contracted T−X−T angles involves constructions utilizing condensed building units which often involve edge sharing tetrahedral condensations or higher coordination numbers. Such condensed building-block construction was observed in the organic templated microporous tin sulfides, SnS-1 ($Sn_3S_7^{2-}$),[150,151] in which all of the tin cations are five coordinate. A second common condensed building block observed in chalcogenide framework construction is the $(M_4X_6)X_4$ adamantine-like unit.[152] These adamantine-like units are most frequently linked into framework structures by ligation of the terminal chalcogenides to divalent transition metals such as in the MGeS-3 frameworks $MGe_4S_{10}^{2-}$.[153] In DPA-GS-8, dipropylammonium-Ge_4S_9, adamantine-like units are linked by bridging terminal chalcogenides $(Ge_4S_6S_2S_{2/2})^{2-}$ to form a zigzag chain.[154] The metrical parameters of an adamantine-like building unit are equivalent to those required for a closest packing arrangement of ions. This requires contracted T−X−T angles making this geometry accessible only for species with longer M−X bonds. Similarly, the edge-shared tetrahedral connectivity in SnS-1 requires contracted T−X−T angles and long T−X bonds to avoid short T−T contacts. Thus, such condensed tetrahedral units are not favored for silicate constructions. Nevertheless, as described above, these metrical parameters are well

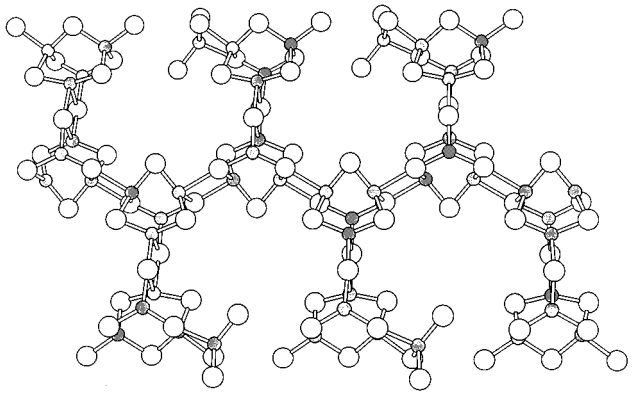

Figure 15. Ball and stick representation of a single complex chain in $[Cu_9Cl_{16}]^{7-}$.

suited for constructions using condensed metal-halide building blocks.

$Cu_9Cl_{16}^{7-}$. Isolated $Cu_4X_6^{2-}$ (X = Br and I) complexes have been known for some time.[155−158] These adamantine-like units exhibit no terminal ligation and are well isolated by large phosphonium and ammonium countercations. Solvothermal synthesis in ethanol utilizing CuCl and the small H_3NMe countercation yielded the first condensed chloride units "Cu_4Cl_6" in which these adamantine building blocks are condensed into a complex chain structure $Cu_9Cl_{16}^{7-}$ with effectively an open-framework pore structure shown in Figure 15.[159] The backbone of this chain structure consists of inner/outer halide bridges linking $Cu_4Cl_4{}^iCl_2{}^{i-a}Cl_2{}^{a-i}$ units. Attached to each backbone complex building unit a second polyanion forms an inner/outer bridge. Further framework condensation is prevented on the pendent polyanion by a terminal chloride and a terminal $CuCl_3$ unit. This "open-framework chain structure" is stabilized by hydrogen-bonding of the ammonium cations to both the polyanionic chain and to an isolated Cl^- anion that resides in the center of this void.

$Cu_7Cl_{11}^{4-}$. A three-dimensional copper-halide open-framework $Cu_7Cl_{11}^{4-}$ (Figure 16) has also recently been prepared from the solvothermal synthesis of $CuCl_2$ in the presence of ethylenediamine.[160] The resulting framework is similarly constructed from condensed copper chloride tetrahedra forming Cu_4Cl_{11} tetramers. These are linked by three $CuCl_{3/3}$ trigonal pyramidal units which surround two $Cu(en)_2^{2+}$ charge-balancing extraframework cations. The four-coordinate $Cu(en)_2^{2+}$ also exhibits weak axial Cu−Cl coordination to the framework. While no direct chalcogenide analogue to this phase is known, the polymorphism of copper(I) chlorides[145] is notably similar to that described for the tin and germanium sulfides[152] such that common principles of framework construction are observed.

Phosphate Analogues. Like silicate framework materials, metal phosphates are of considerable interest for separations and catalysis applications.[12,15,161−164] As an extension of the above silicate analogy, we have demonstrated that $CuCl_4^{3-}$ can function electronically and structurally as a phosphate or thiophosphate analogue for the construction of new metal-halide frameworks. For example, the copper aluminum chloride phases discussed above can be described as $Al(CuCl_4)$ which are electronic and structural analogues of aluminophosphates $Al(PO_4)$.[126] Similarly, the haloz-

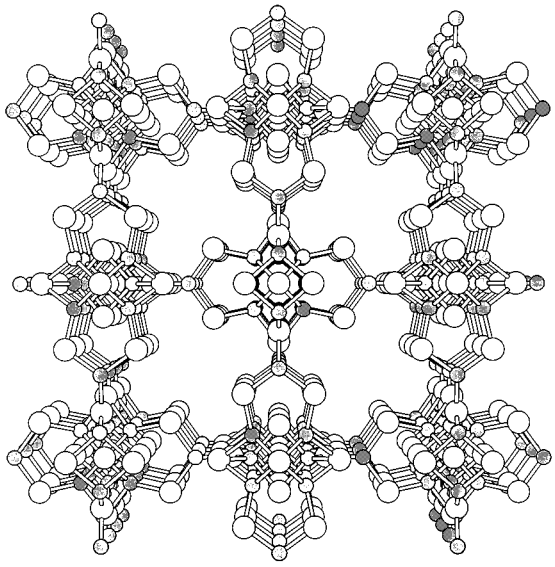

Figure 16. Ball and stick representation of the three-dimensional copper halide open-framework $Cu_7Cl_{11}^{4-}$ viewed down the *c* direction. $[Cu(en)_2]^{2+}$, not shown, fills the channels in this structure.

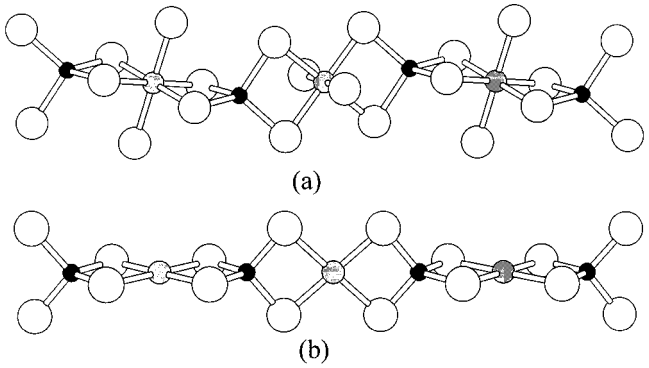

Figure 17. Ball and stick representations illustrating the similarity between the chains found in (a) $[ZrCuCl_6]^-$ and (b) $[NiPS_4]^-$.

eotype copper zinc halides[11] are direct analogues of zinc phosphates; for example, $(ZnPO_4)_3^{3-}$ also adopts the sodalite structure.[135]

$CuZrCl^{6-}$. To further demonstrate this copper chloride/phosphate analogy, we have initiated the synthesis of early transition metal/copper chloride materials with the goal of producing octahedral/tetrahedral framework structures patterned after the extensive family of zirconium, vanadium and molybdenum phosphates. Reaction of CuCl, $ZrCl_4$, and H_2NMe_2Cl in the melt or in a superheated benzene solution (150 °C) yields $[ZrCuCl_6]^-$.[165] This chain structure is constructed from alternating zirconium halide octahedra and copper chloride tetrahedra which share common edges as shown in Figure 17a. The orthogonal orientation of opposing edges of a tetrahedron require the zirconium octahedra to be linked in an orthogonal fashion. In the room-temperature crystal structure, the $ZrCl_6$ unit adopts a nearly ideal octahedral geometry, whereas the copper chloride tetrahedra are significantly distorted due to hydrogen-bonding to the dialkylammonium cations. A phase transition resulting from a reorientation of the alkylammonium cations is observed below 210 K. The $[ZrCuCl_6]^-$ chains are closely related to the $[MPS_4]^-$ chains (M = Ni or Pd)[166,167] in which tetrahedral

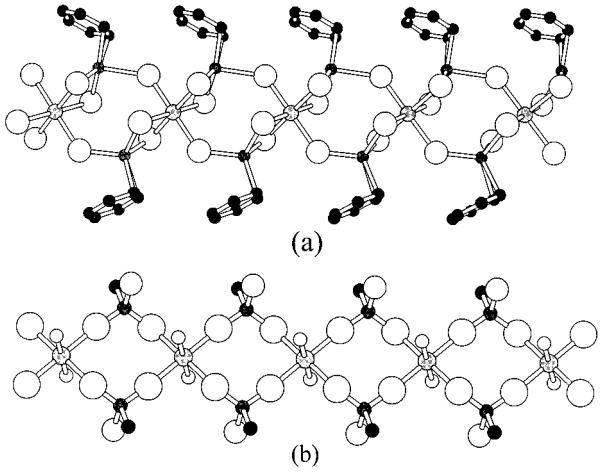

Figure 18. Ball and stick representations illustrating the similarity between the chains found in (a) $((C_6H_6)CuCl_3)_2Zr$ and (b) $[(RPO_3H)_2ZrF_2]^-$, R = $CH_2NH(CH_2CO_2)_2$. The smaller shaded spheres are Cu in (a) and P in (b). The small unshaded spheres represent flourides. Only the methylene carbon of the phosphonate are shown for clarity.

thiophosphate building blocks link square planar metal centers through shared edges (Figure 17b). The tetrahedral building block $CuCl_4^{3-}$ is the charge-matched structural equivalent of PS_4^{3-}, and with the two terminal axial chlorides, $ZrCl_2^{2+}$ is the charge-matched and structural equivalent of the square planar Ni^{2+} or Pd^{2+}. Whereas a notable puckering of the $[ZrCuCl_6]^-$ chain is observed, in the absence of strong hydrogen-bonding, the $[MPS_4]^-$ chains are completely linear with an M−S−S−P dihedral angle of 180°. The long M−X bonds with respect to the size of the metal cations allows an edge shared connectivity observed for the metal copper chloride and metal thiophosphate chains. Short P−O bond distances preclude a similar structure for metal phosphates because of repulsive M−P contacts.

Phosphonate Analogues. Phosphonates, RPO_3^{2-}, are frequently utilized to induce pillared phosphate-type structures in which organic pillars separate inorganic chains or layers.[168−170] A similar pillaring of metal-halide analogues of phosphates might be obtained by utilization of $LCuCl_3^{2-}$ (L = neutral ligand) or $RZnCl_3^{2-}$ (R = alkyl, aryl, ...). Constructions with the $LCuCl_3^{2-}$ phosphonate analogues are particularly attractive for catalytic applications whereby the lability of the Cu−L bond can be exploited to reversibly open a coordination site at a redox active metal center.

$((C_6H_6)CuCl_3)_2Zr$. The solvothermal reaction of CuCl and $ZrCl_4$ in benzene at 150 °C produced yellow crystalline $((C_6H_6)CuCl_3)_2Zr$ for which the structure is shown in Figure 18a.[171] The benzene molecules are coordinated to the copper sites by an η^2-mode of coordination. Two chloride ligands bridge between the copper and equatorial sites on the zirconium octahedron such that a common polyhedral edge is shared. The third chloride is bridged to the apex of the zirconium octahedron. The two $LCuCl_3$ units link zirconium octahedra, related by an approximate center of inversion. Crystal packing of these chains influences unique second-order Jahn−Teller distortions making each of the two $LCuCl_3$ units distinct so as to maximize the edge to face interactions of the aromatic rings in neighboring chains. The benzene can be irreversibly replaced by PPh_3, which also breaks up the chain into $((PPh_3)CuCl_3)_2Zr$ molecular units.[171] A search of the Cambridge Crystallographic Database finds no 1-D phosphonate for which $((C_6H_6)CuCl_3)_2Zr$ is a direct structural analogue. This again is due to the observation that the longer M−Cl distances can readily form edge-bridged contacts, which are rarely seen for the metal oxides. However, the structure of $[(RPO_3H)_2ZrF_2]^-$ (R = $CH_2NH(CH_2CO_2)_2$),[172] shown in Figure 18b, is a very close structural parallel. A figurative loss of 2 equiv of HF would allow for a condensation to an edge-bridged phosphonate which would be a direct analogue to our halide phase.

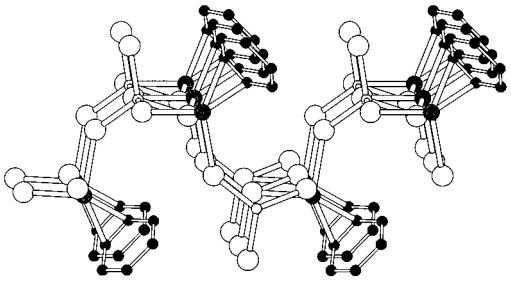

Figure 19. Ball and stick representation looking parallel to the layers of $((C_6H_6)CuCl_3)AlCl$. The smaller shaded spheres are Al and the larger shaded spheres are Cu.

$((C_6H_6)CuCl_3)AlCl$. The same phosphonate analogy is observed for the layered structure of $((C_6H_6)CuCl_3)AlCl$ which is obtained in the reversible adsorption of benzene to $CuAlCl_4$ described above.[130,173] Numerous patents describe the utility of $(C_6H_6)CuAlCl_4$ for the reversible binding and separation of CO from gas mixtures,[174−176] as well as for the catalytic polymerization of olefins[177] and aromatics.[178] Again the benzene molecules are coordinated to the copper sites via an η^2-mode of coordination. As shown in Figure 19, the $LCuCl_3$ units are linked through their corners to aluminum chloride tetrahedra forming an undulating layered structure. Adjacent to each Cu−L bond in the layer is a terminal Al−Cl bond. This is analogous to the molecular species $(({}^tBuPO_3)Al({}^iBu))_4$,[179] which contains the same construction features (a terminal aluminum alkyl replaces the terminal aluminum chloride). The shorter M−O bonds in the aluminophosphonate apparently favor the tetrameric structure as opposed to the undulating layer structure of the copper aluminum halide. The reversible adduct formation of ligands coordinated to $CuAlCl_4$ effectively demonstrates the utility of these construction principles and the potential for such constructions to perform useful chemistry.

Summary

In this review we have described a variety of structural and bonding analogies observed for known metal halide and chalcogenide materials. We have selected structure types for which commonality is observed between halides and chalcogenides, as opposed to emphasizing those structure types for which one and not another set of anions are observed. For example, to date no metal-halide analogues to the copper oxide high-temperature superconductors have been synthesized. But the work described here probes the question: when does nature set limits as to what structure types are accessible for a given set of anions? Such limits are well beyond the boundaries of known chem-

istry. As we have demonstrated, a careful utilization of principles of structure and bonding can provide a rational foundation for the design of new solid-state materials patterned after the vast structural chemistry known for metal oxides. While structural analogies are fundamental to such rational synthesis, the chemical properties of the resulting non-oxide solids are anticipated to be quite varied and useful when applied to diverse applications.

Acknowledgment. This work was supported by the National Science Foundation, CAREER award (DMR-9501370). J. D. Martin is a Cottrell Scholar of the Research Corporation. Though not explicitly referenced, the crystal structure descriptions of Pearson,[18] Wyckoff,[180,181] and the Inorganic Crystal Structure Database and the Cambridge Crystallographic Database were invaluable for writing this manuscript. We also thank X. Bu and G. Stucky for noting the metal-halide ABW-type frameworks observed for $[LiBeF_4]^-$.

Supporting Information Available: Tables containing crystallographic data and positional and isotopic displacement parameters for $[(H_3C)_3N(CH_2)_{15}CH_3]_2Zn_2Cl_6$, $[H_3NCH_3]Cu_2Zn_2Cl_7$, $RbCu_2Zn_2Cl_7$, $[N(CH_3)H_3]_8[Cu_9Cl_{16}][Cl]$, $[N(CH_3)_2H_2]ZrCuCl_6$, and $((C_6H_6)CuCl_3)_2Zr$ (13 pages). See any current masthead page for ordering and Internet access instructions.

References

(1) Cox, P. A. *Transition Metal Oxides: An Introduction to their Electronic Properties*; Clarendon: Oxford, 1992.
(2) Rao, C. N. R. *Transition Metal Oxides*; VCH: New York, 1995.
(3) Lin, G. J.; Miller, J. *Inorg. Chem.* **1993**, *32*, 1476.
(4) Colton, R.; Canterford, J. H. *Halides of the First RowTransition Metals*; Wiley: NewYork, 1968.
(5) Canterford, J. H.; Colton, R. *Halides of the Second and Third RowTransition Metals*; Wiley: New York, 1969.
(6) Brown, D. *Halides of the Lanthanides and Actinides*; Wiley: New York, 1968.
(7) Meyer, G.; Meyer H.-J. *Chem. Mater.* **1992**, *4*, 1157.
(8) Massa, W.; Babel, D. *Chem. Rev.* **1988**, *88*, 275.
(9) Schoonman, J.; Lieth, R. M. A. In *Preparation and Crystal Growth of Materials with Layered Structures*; Lieth, R. M. A., Ed.; D. Reidel: Dordrecht, The Netherlands, 1977; pp 35−69.
(10) Martin, J. D. In *New Directions in Materials Synthesis, ACS Symposium in Print*; Winter, C. H., Hoffman, D. M., Eds.; American Chemical Society: Washington, DC, in press.
(11) Martin, J. D.; Greenwood, K. B. *Angew. Chem., Int. Ed. Engl.* **1997**, *36*, 2072.
(12) Haushalter, R. C.; Mundi, L. A. *Chem. Mater.* **1992**, *4*, 31.
(13) Wells, A. F. *Structural Inorganic Chemistry*, 5th ed.; Oxford: Oxford, 1984.
(14) Meier, W. M.; Olson, D. H. *Atlas of Zeolite Structure Types*; Butterworth-Heinemann: London, 1992.
(15) Feng, P.; Bu, X.; Stucky, G. D. *Nature* **1997**, 388, 735.
(16) West, A. R. *Solid State Chemistry and Its Applications*; Wiley: New York, 1984.
(17) Brese, N. E.; O'Keefe, M. O. *Structure and Bonding*, 79; Springer-Verlag: Berlin, 1992; pp 307−378.
(18) (a) Villars, P.; Calvert, L. D. *Pearsons Handbook of Crystallographic Data for Intermetallic Phases*, 2nd ed.; ASM: Materials Park, OH, 1991; Vols. 1−3.
(19) Martin, J. D.; Corbett, J. D. *Angew. Chem., Int. Ed. Engl.* **1995**, *34*, 233.
(20) Mattheiss, L. F. *Phys. Rev. B* **1974**, 10, 995.
(21) Franzen, H. F. *J. Inorg. Nucl. Chem.* **1966**, 28, 1575.
(22) Svensson, P. H.; Bengtsson-Kloo, L.; Persson, P. *J. Chem. Soc., Dalton Trans.* **1998**, 9, 1425.
(23) Greenwood, N. N.; Earnshaw, A. *Chemistry of the Elements*; Pergamon: London: **1984**, 399.
(24) Schnick, W.; Lücke, J. *Z. Anorg. Allg. Chem.* **1992**, *610*, 121.
(25) Schnick, W.; Lücke, J. *Z. Anorg. Allg. Chem.* **1990**, *588*, 19.
(26) O'Keefe, M. O.; Hyde, B. G. *Acta Crystallogr., Sect. B* **1976**, *32*, 2923.
(27) Angell, C. A.; Wong, J. J. *J. Chem. Phys.* **1970**, *53*, 1053.
(28) Wong, J.; Lytle, F. W. *J. Non-Cryst. Solids* **1980**, 273.
(29) Wright, A. F.; Fitch, A. N.; Wright, A. C. *J. Solid State Chem.* **1988**, *73*, 298.
(30) Narten, A. H. *J. Chem. Phys.* **1972**, *56*, 1905.
(31) Jagner, S.; Helgesson, G. *Adv. Inorg. Chem.* **1991**, *37*, 1.
(32) Brehler, B. *Naturwissenschaften* **1959**, 554.
(33) Oswald, H. R.; Jaggi, H. *Helv. Chim. Acta* **1960**, *43*, 72.
(34) Brehler, B. *Z. Kristallogr.* **1961**, *115*, 373.
(35) Yakel, H. L.; Brynestead, J. *Inorg. Chem.* **1978**, *17*, 3294.
(36) Mueller, H.; Hoppe. R. *Z. Anorg. Allg. Chem.*, **1992**, *611*, 73.
(37) Boisen, M. B., Jr.; Gibbs, G. V.; Bukowinski, M. S. T. *Phys. Chem. Miner.* **1994**, *21*, 269.
(38) Doni, E.; Girlanda, R. In *Electronic Structure and Electronic Transitions for in Layered Materials*; Grasso, V., Ed.; Reidel: Dordrecht, The Netherlands, 1986; 1.
(39) *Structure Phase Transitions in Layered Transition Metal Compounds*; Motizuki, K, Ed.; Reidel: Dordrecht, The Netherlands, 1986.
(40) Canadell, E.; Jobic, S.; Brec, R.; Rouxel, J.; Whangbo, M.-H. *J. Solid State Chem.* **1992**, *99*, 189.
(41) Rovira, C.; Whangbo, M.-H. *Inorg. Chem.* **1993**, *32*, 4094.
(42) Whangbo, M.-H.; Canadell, E. *J. Am. Chem. Soc.* **1992**, *114*, 9587.
(43) Lee, S.; Nagasundaram, N. *Chem. Mater.* **1989**, *1*, 597.
(44) Troyanov, S. I.; Tsyrelnikov, V. I. *Vestn. Mosk. University, Ser. 2: Khim.* **1973**, *67*.
(45) Takeuchi, Y.; Nowacki, W. *Schweiz. Mineral. Petrogr. Mitt.* **1964**, *44*, 105.
(46) Schutte, W. J.; De Boer J. L.; Jellinek, F. *J. Solid State Chem.* **1987**, *70*, 207.
(47) Wilson, J. A.; Di Salvo, F. J.; Mahajan, S. *Phys. Rev. Lett.* **1974**, *32*, 882.
(48) Wilson, J. A.; Di Salvo, F. J.; Mahajan, S. *Adv. Phys.* **1975**, *24*, 117.
(49) Williams, P. M.; Parry, G. S.; Scruby, C. B. *Philos. Mag.* **1974**, *29*, 695.
(50) Williams, P. M. In *Crystallography and Crystal Chemistry of Materials with Layered Structures*; Reidel: Dordrecht, The Netherlands, 1976; Vol. 2, p 51.
(51) Moncton, D. E.; Axe, J. K.; DiSalvo, F. J. *Phys. Rev. B.* **1977**, *16*, 801.
(52) Michaelis, C.; Mattausch, Hj.; Simon, A. *Z. Anorg. Allg. Chem.* **1992**, *610*, 23.
(53) Kasten, A.; Müller, P. H.; Schienle, M. *Solid State Commun.* **1984**, *51*, 919.
(54) Warkentin, E.; Barninghausen, H. *Z. Anorg. Allg. Chem.* **1979**, *459*, 187.
(55) Michaelis, C.; Mattausch, H.; Borrmann, H.; Simon, A.; Cockcroft, J. K. *Z. Anorg. Allg. Chem.* **1992**, *607*, 29.
(56) Murphy, D.; Di Salvo, F. J.; Hull Jr., G. W.; Waszczak, J. W.; Mayer, S. F.; Stewart, G. R.; Early, S.; Acrivos, J. V.; Geballe, T. H. *J. Chem. Phys.* **1975**, *62*, 967.
(57) Takei, H.; Koike, M.; Imai, K.; Sawa, H.; Kadowaki, H.; Iye, Y. *Mater. Res. Bull.* **1992**, *27*, 555.
(58) Goodenough, J. B.; Dutta, G.; Manthiram, A. *Phys. Rev. B.* **1991**, *43*, 10 170.
(59) Brown, B. E. *Acta Crystallogr.* **1966**, *20*, 268.
(60) Rigoult, J.; Guidi-Morosini, C.; Tomas, A.; Molinie, P. *Acta Crystallogr. Sect. B*, **1982**, *38*, 1557.
(61) van Landuyt, J.; Wiegers, G. A.; Amelinck, S. *Phys. Status Solidi A* **1978**, *46*, 479.
(62) Brown, B. E. *Acta Crystallogr.* **1966**, *20*, 264.
(63) Bronsema, K. D.; Bus, G. W.; Wiegers, G. A. *J. Solid State Chem.* **1984**, *53*, 415.
(64) Burrow, J. H.; Maule, C. H.; Strange, P.; Tothill, J. N.; Wilson, J. A. *J. Phys. C. Solid State Phys.* **1987**, *20*, 4115.
(65) Beck, H. P.; Schuster, M. *J. Solid State Chem.* **1992**, *100*, 301.
(66) Warkentin, E.; Bärnighausen, H. *Z. Anorg. Allg. Chem.* **1979**, *459*, 187.
(67) Gal'perin, E. L.; Sandler, R. A. *Kristallografiya* **1962**, *7*, 217.
(68) Reudorff, W.; Becker, H. *Z. Naturforsch., B: Chem. Sci.* **1954**, *9*, 614.
(69) Wypych, F.; Schollhorn, R. *J. Chem. Soc., Chem. Commun.* **1992**, 1386.
(70) Guthrie, D. H.; Corbett, J. D. *J. Solid State Chem.* **1981**, *37*, 256.
(71) Alcock, N. W.; Kjekshus, A. *Acta Chem. Scand.* **1965**, *19*, 76.
(72) Wildervanck, J. C.; Jellinek, F. *J. Less-Common Met.* **1971**, *24*, 73.
(73) Ehrlich, P.; Seifert, H.-J. *Z. Anorg. Allg. Chem.* **1959**, *301*, 282.
(74) Klemm, W.; Grimm, L. *Z. Anorg. Allg. Chem.* **1942**, *249*, 198.
(75) Wells, A. F. *Z. Anorg. Allg. Chem.* **1938**, *100*, 189.
(76) Pinsker, Z. G. *Acta Physicochim.* **1941**, *14*, 503.
(77) Oftedal, I.; Kepustinsky, A. *Z. Phys. Chem.* **1928**, *134*, 301.
(78) van Arkel, A. E. *Physica* **1924**, *4*, 286.
(79) Batsanov, S. S.; Kopaneva, L. I.; Lazareva, E. V. *Russ. J. Inorg. Chem.* **1987**, *32*, 1251.
(80) Meetsma, A.; Wiegers, G. A.; Haange, R. J.; de Boer, J. L. *Acta Crystallogr., Sect. C* **1990**, *46*, 1598.
(81) Bjerkelund, E.; Kjekshus, A. *Acta Chem. Scand.* **1967**, *21*, 513.
(82) Ehrlich, P.; Gutsche, W.; Seifert, H.-J. *Z. Anorg. Allg. Chem.* **1961**, *312*, 80.

(83) Wollan, E. O.; Koehler, W. C.; Wilkinson, M. K. *Phys. Rev.* **1958**, *110*, 638.
(84) Cable, J. W.; Wilkiinson, M. K.; Wollan, E. O.; Koehler, W. C. *Phys. Rev.* **1962**, *125*, 1860.
(85) Tengner, S. *Z. Anorg. Allg. Chem.* **1938**, *239*, 126.
(86) Kjekshus, A.; Rakke, T.; Andresen, A. F. *Acta Chem. Scand.* **1978**, *32*, 209.
(87) Ferrari, A.; Giorgi, F. *Rend. Accad. Lincei.* **1929**, *9*, 1134.
(88) Ferrari, A.; Giorgi, F. *Rend. Accad. Lincei.* **1929**, *10*, 522.
(89) Thomassen, L. *Z. Phys. Chem.* **1929**, *4B*, 277.
(90) Chadha, G. K. *Z. Kristallogr.* **1974**, *139*, 147.
(91) Canadell, E.; Whangbo, M. H. *Chem. Rev.* **1991**, *91*, 965.
(92) van Loon, C. J. J.; Ijdo, D. J. W. *Acta Crystallogr., Sect. B*, **1975**, *31*, 770.
(93) McCarroll, W. H.; Katz, L.; Ward, R. *J. Am. Chem. Soc.* **1957**, *79*, 5410.
(94) Hinz, D J.; Meyer, G.; Dedecke, T.; Urland, W. *Angew. Chem. Intl. Ed. Engl.* **1995**, *34*, 71.
(95) Seo, D.-K.; Whangbo, M.-H. *J. Am. Chem. Soc.* **1996**, *118*, 3951.
(96) Siepmann, R.; von Schnering, H. G.; Schäfer, H. *Angew. Chem.* **1967**, *79*, 650.
(97) von Schnering, H. G.; May, W.; Peters, K. *Z. Kristallogr.* **1993**, *208*, 368.
(98) Cotton, F. A.; Mague, J. T. *Inorg. Chem.* **1964**, *3*, 1402.
(99) Corbett, J. D. In *Modern Perspectives in Inorganic Crystal Chemistry*; Parthe, E. Ed.; Kluwer: Norwell MA, 1992.
(100) Mingos, D. M. P.; Wales, D. J. *Introduction to Cluster Chemistry*; Prentice Hall: Englewood Cliffs, NJ, 1990.
(101) Simon, A. *Angew. Chem., Int. Ed. Engl.* **1988**, *27*, 159.
(102) Bronger, W.; Kanert, M.; Loevenich, D. S.; Schwochau, K. *Angew. Chem., Int. Ed. Engl.* **1993**, *32*, 576.
(103) Lee, S. C.; Holm, R. H. *Angew. Chem., Int. Ed. Engl.* **1990**, *29*, 840.
(104) von Schnering, H. G.; Schäfer, H. *Angew. Chem.* **1964**, *76*, 833.
(105) Hwu, S.-J.; Corbett, J. D. *J. Solid State Chem.* **1986**, *64*, 331.
(106) Toradi, C. C.; McCarley, R. E. *J. Am. Chem. Soc.* **1979**, *101*, 3963.
(107) Cordier, S.; Perrin, C.; Sergent. M. *Mater. Res. Bull.* **1997**, *32*, 25.
(108) Cordier, S.; Perrin, C.; Sergent. M. *Eur. J. Solid State Inorg. Chem.* **1994**, *31*, 1049.
(109) Bauer, D.; von Schnering, H.-G. *Z. Anorg. Allg. Chem.* **1968**, *361*, 259.
(110) von Schnering, H.-G. *Z. Anorg. Allg. Chem.* **1971**, *385*, 75.
(111) Fenske, D., Hachgenei, J.; Ohmer, J. *Angew. Chem., Int. Ed. Engl.* **1985**, *24*, 706.
(112) Simon, A.; von Schnering, H. G.; Wöhrle, H.; Schäfer, H. *Z. Anorg. Allg. Chem.* **1965**, *339*, 155.
(113) Boschen, S.; Keller, H.-L.; von Schnering, H. G. *Z. Kristallogr.* **1991**, *196*, 159.
(114) Schäfer, H.; von Schnering, H. G.; Tillack, J.; Kuhnen, F.; Woehrle, H.; Baumann, H. *Z. Anorg. Allg. Chem.* **1967**, *353*, 281.
(115) Chen, S.; Robinson, W. R. *J. Chem. Soc., Chem. Commun.* **1978**, 879.
(116) Simon, A.; von Schnering, H. G.; Schäfer, H. *Z. Anorg. Allg. Chem.* **1967**, *355*, 295.
(117) Bronger, W.; Miessen, H.-J.; Müller, P.; Neugroschel, R. *J. Less-Common Metals* **1985**, *105*, 303.
(118) Dudis, D. S.; Corbett, J. D. *Inorg. Chem.* **1987**, *26*, 1933.
(119) Burnus, R., Köhler, J.; Simon, A. *Z. Naturforsch.* **1987**, *B42*, 536.
(120) Simon, A. *Angew. Chem., Int. Ed. Engl.* **1988**, *27*, 159.
(121) Leduc, L.; Perrin, A.; Sergent, M. *Comput. Rend. Acad. Sci (Paris), Ser. II* **1983**, *296*, 961.
(122) Hughbanks, T.; Corbett, J. D. *Inorg. Chem.* **1989**, *28*, 631.
(123) Lii K. H.; Wang C. C.; Wang S. L. *J. Solid State Chem.* **1988**, *77*, 407.
(124) Bateman, L. R.; Blount J. F.; Dahl, L. F. *J. Am. Chem. Soc.* **1966**, *88*, 1082.
(125) Potel, M.; Gougeon, P.; Chevrel, R.; Sergent, M. *Rev. Chim. Miner.* **1984**, *21*, 509.
(126) Martin, J. D.; Leafblad, B. R.; Sullivan, R. M.; Boyle, P. D. *Inorg. Chem.* **1998**, *37*, 1341.
(127) Burus, R.; Zajonc, A.; Meyer, G. *Z. Kristallogr.* **1995**, *210*, 62.
(128) Hildebrandt, L.; Jones, P. G.; Schwarzmann, E.; Sheldrick, G. M. *Z. Naturforsch., B: Chem. Sci.* **1986**, *33*, 1978.
(129) Yamada, K.; Tomita, Y.; Okuda, T. *J. Mol. Struct.* **1995**, *345*, 219.
(130) Turner, R. W.; Amma, E. L. *J. Am. Chem. Soc.* **1966**, *88*, 1877.
(131) Martin, J. D.; Sullivan, R. M. Unpublished results.
(132) Sullivan R. M.; Martin, J. D.; Liu, H.; Ciroala, M.; Grey, C. P.; Hanson, J. Unpublished results.
(133) Gable, R W.; Hoskins, B. F.; Robson, R. *J. Chem. Soc., Chem. Commun.* **1990**, 762.
(134) Depmeier, W. *Acta Crystallogr., Sect. B*, **1984**, *40*, 185−191. $a = 4\ l\ (\sin(\alpha/2)\cos(\phi) + \cos(\alpha/2))$.
(135) Nenoff, T. M.; Harrison, W. T. A.; Gier, T. E.; Keder, N. L.; Zaremba, C. M.; Srdanov, V. I.; Nicol, J. M.; Stucky, G. D. *Inorg. Chem.* **1994**, *33*, 2472.
(136) Chung, S. J.; Hahn, Th. *Mater. Res. Bull.*, **1972**, 7, 1209.
(137) Anderson, M. R.; Brown, I. D.; Vilminot, S. *Acta Crystallogr., Sect. B* **1973**, *29*, 2625.
(138) Bu, X.; Feng, P.; Thurman, E. G.; Stucky, G. D. *Zeolites* **1997**, *19*, 200.
(139) le Roy, J.; Aleonard, S. *Acta Crystallogr., Sect. B* **1982**, *24*, 1968.
(140) Perrotta, A. J.; Smith, S. M.; Smith, J. V. *Mineral. Magn. J. Mineral. Soc.* **1965**, *35*, 588.
(141) Beck, J. S.; Vartuli. J. C.; Roth, W. J.; Leonowicz, M. E.; Kresge, C. T.; Schmitt, K. D.; Chu, C. T.-W.; Olson, D. H.; Sheppard, E. W.; McCullen, S. B.; Higgins, J. B.; Schlenker, J. L. *J. Am. Chem. Soc.* **1992**, *114*, 10834.
(142) Corma, A. *Chem. Rev.* **1997**, *97*, 2373.
(143) Thornton, T. A.; Martin, J. D. To be submitted.
(144) Li, J.; Marler, B.; Kessler, H.; Soulard, M.; Kallus, S. *Inorg. Chem.* **1997**, *36*, 4697.
(145) Zuniga, F. J.; Gervais, Chapuis *Cryst. Struct. Commun.* **1981**, *10*, 533.
(146) Eisenmann, B.; Jakowski, M.; Klee, W.; Schaefer, H. *Rev. Chim. Min.* **1983**, *20*, 255.
(147) Greenwood, K. B.; Euliss, L. E.; Martin, J. D. To be submitted.
(148) Eisenmann, B.; Jakowski, M.; Klee, W.; Schaefer, H. *Rev. Chim. Min.* **1983**, *20*, 329.
(149) Perloff, A.; Block, S. *Acta Crystallogr.* **1966**, *20*, 274.
(150) Bedard, R. L.; Vail, L. D.; Wilson, S. T.; Bennett, J. M.; Flanigen, E. M. *Studies in Surface Science and Catalysis, Proc. 8 Int. Zeolite Conf.* **1989**, *49*, 375.
(151) Parise, J. B.; Ko, Y.; Rijssenbeek, J.; Nellis, D. U.; Tan, K.; Kock, S. *J. Chem. Soc., Chem. Commun.* **1994**, 527.
(152) Bowes, C. L.; Ozin, G. A. *Adv. Mater.* **1996**, *8*, 13 and references therein.
(153) Yaghi, O. M.; Sun, Z.; Richardson, D. A.; Groy, T. L. *J. Am. Chem. Soc.* **1994**, *116*, 807.
(154) Nellis, D. M.; Ko, Y.; Tan, K.; Koch, S.; Parise, J. B. *J. Chem. Soc., Chem. Commun.* **1995**, 541.
(155) Asplund, M.; Jagner, S. *Acta Chem. Scand.* **1984**, *A38*, 725.
(156) Andersson, S.; Jagner, S. *Acta Chem. Scand.* **1986**, *A40*, 210.
(157) Bowmaker, G. A.; Clark, G. R.; Yuen, D. K. P. *J. Chem. Soc., Dalton Trans.* **1976**, 2329.
(158) Rath, N. P.; Holt, E. M. *J. Chem. Soc., Chem. Commun.* **1985**, 665.
(159) Yang, J.; Martin, J. D. To be submitted.
(160) DeBord, J. R. D.; Lu, Y.; Warren, C.; Haushalter, R. C.; Zubieta, J. *J. Chem. Soc.* **1997**, 1365.
(161) Wilson, S. T.; Lok, B. M.; Messina, C. A.; Cannan, T. R.; Flanigen, E. M. *ACS Symp. Ser.* **1983**, 218.
(162) Nataragan, S.; Attfield, M. P.; Cheetham, A. K. *Angew. Chem., Int. Ed. Engl.* **1997**, *36*, 978.
(163) Alberti, G.; Casciola, M.; Constantino, U.; Vivani, R. *Adv. Mater.* **1996**, *8*, 291.
(164) Centi, G.; Trifirò, F.; Ebner, J. R.; Franchetti, V. M. *Chem. Rev.* **1988**, *88*, 55.
(165) Dattelbaum A. M.; Martin, J. D. To be submitted.
(166) Elder, S. H.; Van der Lee, A.; Brec, R.; Canadell, E. *J. Solid State Chem.* **1995**, *116*, 107.
(167) Chondoudis, K.; Kanatzidis, M. G.; Sayettat, J.; Jobic, S.; Brec, R. *Inorg. Chem.* **1997**, *36*, 5859.
(168) Clearfield, A. *Acc. Chem. Res.* **1988**, *88*, 125.
(169) Thompson, M. *Chem. Mater.* **1994**, *6*, 1168.
(170) Cao, G.; Hong, H.; Mallouk, T. E. *Acc. Chem. Res.* **1992**, *25*, 420.
(171) Dattelbaum, A. M.; Martin, J. D. To be submitted.
(172) Zhang, L.; Poojary, D. M.; Clearfield, A. *Inorg. Chem.* **1998**, *37*, 249.
(173) Martin, J. D.; Leafblad, B. R.; Sullivan, R. M. To be submitted.
(174) Haase, D. J.; Walker, D. G.; Ostrowski, P. C. Gas separation using liquid sorbents containing bimetallic salt complexes and alkylation inhibitors. U.S. Patent 171,630, July 1980.
(175) Yoshida, H.; Watabe, K.; Mukai, K.; Suzuki, I.; Azua, S. Continuous separation of carbon monoxide. Jpn. Patent 60,215,-512, Oct 28, 1985.
(176) Azuma, S.; Asaoka, S.; Kaita, J.; Suzuki, I. Recovery of high-purity carbon monoxide. Jpn. Patent 61,122,111, June 10, 1986.
(177) Johnson, B. H. Catalysis for the Polymerization of Olefins to Yield Predominantly Dimers and Trimers. U.S. Patent 3,475,-347, Nov 16, 1966.
(178) Hara, S.; Toshima, N. *J. Electroanal. Chem.* **1994**, *379*, 181.
(179) Yang, Y.; Schmidt, H.-G.; Noltemeyer, M.; Pinkas, J.; Roesky, H. W. *J. Chem. Soc., Dalton Trans.* **1996**, 3609.
(180) Wyckoff, R. W. G. *Crystal Structures*; Interscience: New York, 1948; Vol. 1.
(181) Wyckoff, R. W. G. *Crystal Structures*; Interscience: New York, 1951; Vol. II.

CM9802550